Morphometry of Hilar Ectopic Granule Cells in the Rat

Joseph P. Pierce,[1]* Daniel P. McCloskey,[2] and Helen E. Scharfman[3,4]

[1]Division of Neurobiology, Department of Neurology and Neuroscience, Weill Cornell Medical College, New York, New York 10065
[2]Department of Psychology and Program in Developmental Neuroscience, College of Staten Island, CUNY, Staten Island, New York 10314
[3]Center for Dementia Research, Nathan Kline Institute, Orangeburg, New York 10962
[4]Department of Child & Adolescent Psychiatry, Psychiatry, Physiology & Neuroscience, New York University Langone Medical Center, New York, New York 10021

ABSTRACT

Granule cell (GC) neurogenesis in the dentate gyrus (DG) does not always proceed normally. After severe seizures (e.g., status epilepticus [SE]) and some other conditions, newborn GCs appear in the hilus. Hilar ectopic GCs (EGCs) can potentially provide insight into the effects of abnormal location and seizures on GC development. Additionally, hilar EGCs that develop after SE may contribute to epileptogenesis and cognitive impairments that follow SE. Thus, it is critical to understand how EGCs differ from normal GCs. Relatively little morphometric information is available on EGCs, especially those restricted to the hilus. This study quantitatively analyzed the structural morphology of hilar EGCs from adult male rats several months after pilocarpine-induced SE, when they are considered to have chronic epilepsy. Hilar EGCs were physiologically identified in slices, intracellularly labeled, processed for light microscopic reconstruction, and compared to GC layer GCs, from both the same post-SE tissue and the NeuroMorpho database (normal GCs). Consistently, hilar EGC and GC layer GCs had similar dendritic lengths and field sizes, and identifiable apical dendrites. However, hilar EGC dendrites were topologically more complex, with more branch points and tortuous dendritic paths. Three-dimensional analysis revealed that, remarkably, hilar EGC dendrites often extended along the longitudinal DG axis, suggesting increased capacity for septotemporal integration. Axonal reconstruction demonstrated that hilar EGCs contributed to mossy fiber sprouting. This combination of preserved and aberrant morphological features, potentially supporting convergent afferent input to EGCs and broad, divergent efferent output, could help explain why the hilar EGC population could impair DG function. J. Comp. Neurol. 519:1196–1218, 2011.

INDEXING TERMS: dentate gyrus; hilus; epilepsy; seizures; hippocampus; pilocarpine

In the dentate gyrus (DG), the primary principal cells are the granule cells (GCs), which form a densely-packed cell layer with highly organized dendrites and axons (Golgi, 1886; Cajal, 1909; Lorente de Nó, 1934). The laminar specificity of this pattern of organization has been described in detail (Amaral et al., 2007; Frotscher et al., 2007; Witter, 2007) and is a signature characteristic of the DG. DG laminar specificity is also normally preserved into adulthood, which is remarkable given that GCs are born throughout life (Gould and Cameron, 1996; Gage et al., 1998) and must migrate into the GC layer accurately, even when cues that regulate migration in development are no longer present.

Notably, some GCs do develop outside of the normal GC layer, at ectopic locations such as the hilus (Amaral and Woodward, 1977; Amaral, 1978; Gaarskjaer and Laurberg, 1983; Marti-Subirana et al., 1986; Seress et al., 1991; for review, see Scharfman et al., 2007) and even

Grant sponsor: National Institutes of Health (NIH); Grant number: NS 41490; Grant sponsor: New York State Department of Health and Office of Mental Health.

*CORRESPONDENCE TO: Dr. Joseph P. Pierce, Division of Neurobiology, Department of Neurology and Neuroscience, Weill Cornell Medical College, 407 E. 61st St., Rm. 408, New York, NY 10065.
E-mail: jppierc@med.cornell.edu

Received June 14, 2010; Revised October 14, 2010; Accepted December 10, 2010
DOI 10.1002/cne.22568
Published online December 23, 2010 in Wiley Online Library (wileyonlinelibrary.com)

area CA3 (Szabadics et al., 2010). Hilar ectopic GCs (EGCs) are usually rare, and not considered to have a major role in the function of the DG (Scharfman et al., 2007). However, pathological conditions that disrupt postnatal neurogenesis can greatly enhance the size of this population. For example, severe continuous seizures (status epilepticus [SE]) in rodents lead to a dramatic increase in GC proliferation (Bengzon et al., 1997; Parent et al., 1997). Many of these cells are thought to mis-migrate to the hilus because levels of reelin, a normal "stop" signal secreted by hilar cells, decline when vulnerable portions of the reelin-expressing cell population in the hilus die in response to SE (Gong et al., 2007). Hilar EGCs could also develop for other reasons (Li and Pleasure, 2005). Regardless of the mechanisms associated with their formation, a large population of EGCs accumulate in the hilus, in days to weeks after SE (Parent et al., 1997; Scharfman et al., 2000, 2007; Scharfman, 2004; McCloskey et al., 2006; Walter et al., 2007; Jessberger et al., 2007b).

The population of hilar EGCs that develop after SE are of particular interest because they survive for long periods of time (McCloskey et al., 2006; Jessberger et al., 2007b) and appear to predispose the DG and CA3 regions to synchronize abnormally (Scharfman et al., 2000, 2007; Scharfman, 2004), which could contribute to abnormal excitability. In support of this hypothesis, drugs that decrease the number of hilar EGCs also lead to a reduction in subsequent seizures (although these drugs have additional actions, potentially also effecting seizures long-term) (Jung et al., 2004, 2006). However, some manipulations that decrease the proliferation of newborn GCs after SE do not appear to ameliorate the chronic seizures that follow, although cognitive deficits are improved (Pekcec et al., 2008). Thus, animal studies indicate that hilar EGCs may have an influence on seizures, or the cognitive impairments associated with limbic seizures (Scharfman and Gray, 2007; Kuruba and Shetty, 2007; Parent and Murphy, 2008; Danzer, 2008).

Further support for the potential importance of hilar EGCs comes from their identification in human tissue specimens from patients with pharmacoresistant temporal lobe epilepsy (TLE) (Parent et al., 2006). However, it should be noted that some of these hilar EGCs are located quite close to the GC layer, raising the possibility that they could result from a general dispersion of GC layer GCs induced by depleted reelin levels (Haas and Frotscher, 2010), rather than the mis-migration of newborn GCs. Indeed, evidence for robust proliferation in human TLE, which could potentially lead to significant hilar EGC formation, is not strong (Blumcke et al., 2001), while data in support of dispersion is (Scheibel et al., 1974; Houser, 1990; Thom et al., 2002). Additionally, there is evidence supporting proliferation at early ages, or in the early phases of epileptogenesis (Blumcke et al., 2002; Scharfman and Gray, 2007).

Hilar EGCs are also intriguing because they allow one to ask how much of the structure and function of GCs depends on their position within the DG. Analysis of hilar EGCs from animals that had SE indicated that, despite the history of seizures, some of the characteristics of hilar EGCs were comparable to those of normal GC layer GCs. For example, the intrinsic membrane properties and firing behavior of normal GC layer GCs and hilar EGCs were extremely similar (Scharfman et al., 2000), although recent studies have identified some differences, such as a more depolarized resting potential in hilar EGCs (Zhan and Nadler, 2009). In contrast, the dendritic morphology of many hilar EGCs appeared to differ qualitatively from that of typical GC layer GCs, with hilar EGCs displaying a bipolar or multipolar structure compared to unipolar GC layer GCs (Scharfman et al., 2000; Ribak et al., 2000; Jessberger et al., 2007b; Walter et al., 2007; Shapiro et al., 2008).

This study was therefore conducted to quantitatively determine the extent to which the morphological structure of the dendrites and axons of hilar EGCs differs from those of GC layer GCs. Hilar EGCs were: 1) identified and physiologically characterized in hippocampal slices from pilocarpine-treated rats which subsequently displayed spontaneous recurrent stage 5 convulsions (i.e., were epileptic); 2) intracellularly injected with Neurobiotin, processed for light microscopic (LM) analysis; and 3) reconstructed, to allow a quantitative characterization of dendritic and axonal arborization. Hilar EGCs were then compared to GC layer GCs, either derived from comparable tissue, or obtained from the NeuroMorpho database (http://NeuroMorpho.Org; Ascoli et al., 2007) as reconstructions of GC layer GCs from normal rats. The findings provide new information about the ways GC development is influenced by the local environment, abnormal excitability, and for the interpretation of DG reorganization in animal models that use SE to study the pathogenesis of TLE.

MATERIALS AND METHODS

Subjects

Animal care and use was in accordance with the guidelines set by the National Institutes of Health and the New York State Department of Health. Adult male Sprague-Dawley rats (Taconic Farms; Germantown, NY) were housed 2–3/cage using a 12-hour light:dark cycle and both standard rat chow (Purina 5001, W.F. Fisher, Summerville, NJ) and water were provided ad libitum.

Pilocarpine administration to induce SE

At 39.1 ± 1.2 days of age (range: 31–43 days) and 212.1 ± 5.1 g body weight (range: 190–230 g), animals were injected with atropine methylbromide (1 mg/kg subcutaneously [s.c.]), followed 30 minutes later by pilocarpine hydrochloride (380 mg/kg, intraperitoneally [i.p.]). SE was defined as the first stage 4–5 seizure (stage 4: rearing and bilateral forelimb clonus; stage 5: the same, followed immediately by loss of postural control; Racine, 1972) that did not terminate. Instead, the stage 4–5 seizure was followed by continual tonic-clonic movements of the head, torso, and/or tail, typically small trembling-like movements of the entire body, in a prone position. SE typically began within 1 hour of pilocarpine injection and was preceded by intermittent stage 1–5 seizures that self-terminated (i.e., normal behavior resumed, such as grooming).

One hour after the onset of SE, animals received an injection of diazepam (5 mg/kg, i.p.), to decrease the severity of SE. After diazepam injection, tonic-clonic movements were attenuated but did not completely stop until 5–6 hours later. Approximately 6 hours after the start of SE, animals received an injection of 5% dextrose in lactate-Ringers solution (2.5 mL, s.c.) to ensure adequate hydration during recovery from SE. In addition, halves of apple were positioned near the animal once each day for 3–5 days after SE. Control rats were treated identically, i.e., they received atropine methylbromide, diazepam, and lactate-Ringers solution, apple, etc., but they were administered an equivalent volume of phosphate-buffered saline (pH 7.4) s.c. instead of pilocarpine.

Slice preparation and maintenance

Animals were deeply anesthetized and immediately decapitated. The brain was rapidly removed and immediately immersed in ice-cold artificial cerebrospinal fluid (ACSF), with sucrose used instead of NaCl (sucrose-ACSF; in mM: 126 sucrose, 5 KCl, 2.0 $CaCl_2$, 2.0 $MgSO_4$, 26 $NaHCO_3$, 1.25 NaH_2PO_4, and 10 d-glucose; pH 7.4). Slices (400 μm thick) were cut through the hippocampus and entorhinal cortex in the horizontal plane using a Vibroslice (Campden Instruments, Lafayette, IN) and immediately transferred to oxygenated sucrose-ACSF at room temperature. Within 5 minutes all slices were transferred to a nylon net in a recording chamber, where they were maintained at an interface of sucrose-ACSF and warm (31–33°C), humidified air (95% O_2, 5% CO_2). The chamber was based on an interface design previously supplied by Fine Science Tools (Foster City, CA), but modified to increase humidity in the compartment where slices were placed, and to allow slices to be submerged up to their surface. Flow of ACSF was controlled by a peristaltic pump (Minipuls 2, Gilson, Worthington, OH) at ≈1 mL/min. Thirty minutes after slices were placed in the chamber, sucrose-ACSF was switched to ACSF containing 126 mM NaCl instead of sucrose (NaCl-ACSF). Recordings began 30 minutes thereafter and were stopped ≈3 hours after the dissection.

Electrophysiology

Recording

Intracellular recordings were made with borosilicate glass with a capillary in the lumen (0.75 mm i.d., 1.0 mm o.d.; World Precision Instruments, New Haven, CT), filled with 4% Neurobiotin (Vector, Burlingame, CA) in 1 M potassium acetate. Resistance was 60–80 megaohms. Extracellular recordings from the area CA3b cell layer were made with electrodes that were 5–10 megaohms and filled with NaCl-ACSF. Intracellular data were collected using an intracellular amplifier with a bridge circuit (Axoclamp 2B, Molecular Devices, Palo Alto, CA), and the bridge was balanced whenever current was passed. Data were collected using a digital oscilloscope (Pro10, Nicolet Instruments, Madison, WI) and analyzed with accompanying Nicolet software and Origin v. 7.5 (OriginLabs, Northampton, MA).

Stimulation

Electrical stimulation used a monopolar stimulating electrode made from Teflon-coated stainless-steel wire (75 μm diameter, including the Teflon coating). Stimuli were triggered digitally (10–200 μs; Pulsemaster, World Precision Instruments) using a stimulus isolator (100 μA; AMPI Instruments, Jerusalem, Israel). For stimulation of the perforant path, the stimulating electrode was placed on the fibers of the perforant path axons, where they converge as they enter the DG (Scharfman et al., 2002).

Evaluation of hilar EGCs

Recordings were made from cells that were identified electrophysiologically as GCs (Scharfman et al., 2000). Electrophysiological characteristics that were used to define GCs were based on intrinsic properties and firing behavior, which were characterized using intracellularly injected current steps (±0.05–1.0 nA, 200 ms), similar to previous studies (Scharfman, 1995a; Scharfman et al., 2000). In brief, the defining features of GCs included: 1) an action potential (AP) with a maximal rising slope that was greater than the maximal slope of the decay phase, when evoked at threshold or when the cell was depolarized so it fired spontaneously; 2) spike frequency adaptation in response to injected current commands; 3) a triphasic spike afterhyperpolarization following an AP at threshold, evoked using a current command (200 ms pulse duration) or when the cell was depolarized and spikes occurred

spontaneously (see Results). These characteristics were chosen because they helped distinguish GCs from other cell types in the DG in past studies with similar methods (Scharfman, 1992, 1995a; Scharfman et al., 2000).

Intracellular labeling and processing

After recordings were completed, cells were injected with Neurobiotin as described previously (Scharfman, 1995b; Scharfman et al., 2000). Repetitive depolarizing current pulses ($^{+}$0.30–0.50 nA, 20 ms, 30 Hz) were delivered for a total of 5–10 minutes. After dye injection (15–60 minutes after the end of current injection), the slice was removed from the recording chamber, placed flat in a Petri dish, covered with filter paper, and immersed in a fixative (2% acrolein, Polysciences, Warrington, PA) and 2% paraformaldehyde in 0.1 M phosphate buffer (PB; pH 7.4). Acrolein, as the most rapidly penetrating of the aldehyde fixatives (Sabatini et al., 1964), provides superior preservation of fine structure when immersion fixation is required (Takahashi et al., 2002). After 3 hours, they were transferred to 0.1 M PB, then to a storage solution (30% sucrose and 10% ethylene glycol in 0.1 M PB) at 4°C. After 1–2 days, each slice was embedded in 4% agar and sectioned using a Vibratome (40 μm; Vibratome 1000; Ted Pella, Redding, CA) and the order of sections was noted for subsequent reconstruction after tissue processing. Sections were washed in 0.1 M Tris buffer, pH 7.4 (3 × 5 minutes), incubated in ABC (ABC Standard Kit, Vector Labs) in Tris (2 hours), washed in Tris (3 × 5 minutes), incubated in diaminobenzidine (Polysciences; 50 mg/100 mL Tris) until the cell could be fully visualized (10–30 minutes), and washed in Tris (3 × 5 minutes). Sections were then either mounted on glass slides or further processed. Further processing for future correlated analysis involved: 1) postfixation in 2% osmium for 1 hour; 2) dehydration (70% ethanol, 3 minutes; 90% ethanol, 5 minutes; 95% ethanol, 10 minutes; 100% ethanol, 15 minutes; 100% ethanol, 15 minutes); 3) incubation in 1:1 Embed 812 (Electron Microscopy Sciences, Fort Washington, PA) and propylene oxide for 12 hours; 4) embedding in Embed 812 between Aclar film (Allied Signal, Pottsville, PA); and 5) polymerization at 60°C for 72 hours.

Cell reconstruction and analysis

Sections were examined at the LM level and all dendritic and axonal processes were hand-traced onto individual tracing paper sheets using a 40× objective and a camera lucida attachment. In addition, select portions (≈50 μm in length) of proximal (primary and secondary) and distal (terminal and next to terminal) dendritic branches were traced using a 100× oil objective for spine analysis (measured in terms of spines/μm). Tracings of consecutive sections were then aligned using cut dendritic and axonal ends. Manual reconstructions were used to guide computer reconstruction using Neurolucida 8 (MicroBrightField, Colchester, VT). Reconstructed cells were then analyzed using Neurolucida Explorer 8 in terms of: 1) total and individual dendritic length (in μm); 2) total and individual dendritic field size (using a 3D convex hull analysis, in μm^3); 3) total and individual dendritic branch node number; 4) average dendritic internodal distance (in μm); 5) dendritic branching pattern (quantified with vertex analysis, which uses topological and metric parameters to characterize the symmetry of branching; Sadler and Berry, 1983); and 6) total axonal length (in μm), and to generate images of the cells rotated 90° from the plane of sectioning. Micrographs and illustrations were prepared in Adobe Photoshop CS3 (San Jose, CA). Micrographs were adjusted in terms of both their levels and focus to improve the quality of the image.

Statistics

The statistical significance between groups was analyzed using Student's *t*-tests. *P*-values <0.05 were considered significant. Values are reported as mean ± SEM, with SEM values rounded to one significant digit. Cluster analysis was also used (SPSS, Chicago, IL).

RESULTS

Sample populations

Twenty-one presumptive EGCs in slices from 17 animals were injected with Neurobiotin and processed for LM. Of these, seven EGCs (798-2, 889-3, 906-2, 910-1, 910-2, 913-3, 917-2) from six animals were selected for reconstruction and analysis (Tables 1, 2), based on the quality of the Neurobiotin fill and their physiological characterization (these reconstructions will be submitted to NeuroMorpho.org). Six of the EGCs were from pilocarpine-injected animals that displayed spontaneous seizures, and one (889-3) was from a saline-injected control animal. All but one of the pilocarpine-injected animals were euthanized at ages ranging from 3.5–7 months of age (weighing 180–230 g), 3–6 months after SE, when acute changes following pilocarpine-induced SE would have long since passed, and slices of most animals exhibit spontaneous, rhythmic, epileptiform burst discharges in area CA3 (Scharfman et al., 2000). The remaining animal (which yielded cell 906-2) was euthanized at 12.5 months of age, 11 months after SE. The EGC from this animal (906-2) was also distinct in that it was recorded in a slice from the dorsal half of the hippocampal formation, whereas all of the other cells were recorded in slices originating from the ventral half.

Five of the six EGCs from pilocarpine animals had cell bodies that were positioned relatively centrally within the

TABLE 1.
Anatomical Data for Each Cell

Cell	Type	Arbor Region	Dend #	Node #	Dend L (μm)	L/Node (μm)	Convex Hull (x10^6 μm^3)	% C	Axon L (μm)	Axon Arbor Region
798-2	HE E	Hilus	4	15	3020	201	2.54	16	x	x
910-1	HE E	Hilus	3	19	3863	203	5.87	86	6715	CA3, ML, hilus
910-2	HE E	Hilus	2	17	2498	147	1.96	33	6823	CA3, ML, hilus
913-3	HE E	Hilus	2	22	3312	151	6.20	75	6784	CA3, ML, hilus
917-2	HE E	Hilus	3	22	3666	167	4.26	100	2127	CA3, ML, hilus
906-2	E	H + ML	4	11	3116	283	3.12	10	x	x
889-3	C E	H + ML	3	16	2029	127	1.15	46	x	x
3319201	N GCL	ML	2	18	4903	272	10.9	100	x	x
3319202	N GCL	ML	1	15	4239	283	6.01	100	x	x
404881	N GCL	ML	2	13	2866	220	3.82	100	x	x
5199202	N GCL	ML	1	18	4995	278	7.57	100	x	x
523886	N GCL	ML	2	11	3156	287	5.28	100	x	x
524892a	N GCL	ML	1	14	3704	265	5.51	100	x	x
524892b	N GCL	ML	1	12	3086	257	3.04	100	x	x
609885	N GCL	ML	1	14	3592	257	5.49	100	x	x
614882	N GCL	ML	2	15	3181	212	5.97	100	x	x
B106885	N GCL	ML	2	14	3838	274	4.43	100	x	x
B330886	N GCL	ML	1	12	3485	290	4.25	100	x	x
916-1	PS GCL	H + ML	3	20	4228	211	6.61	70	x	x
124-5R	PS GCL	ML	1	18	3694	205	5.15	78	x	x
124-5L	PS GCL	ML	2	13	3519	271	4.23	82	x	x
103-5	PS GCL	H + ML	2	10	2889	289	5.68	92	x	x

Summary table of the anatomical data from hilar EGCs and GC layer GCs. Data from hilar EGCs (EGC 798-2 through 889-3), normal GC layer GCs (obtained from the NeuroMorpho data base, 3319201 through B330886) and post-SE GC layer GCs (916-1 through 103-5). HE E, hilar-exclusive ectopic GC. E, ectopic GC. C E, control ectopic GC. N GCL, normal GC layer GC. PS GCL, post-SE GC layer GC. H + ML, hilus and molecular layer. ML, molecular layer. Dend #, number of dendrites per cell. Node #, number of dendritic branch points (nodes) per cell. Dend L, total dendritic length per cell. L/Node, average internodal distance. Convex Hull, 3D Convex Hull analysis. % C, percentage of dendritic endings that were complete. Axon L, total axonal length per cell.

hilus and dendritic arbors that were exclusively, or almost exclusively, restricted to the hilus. Four of these cells (910-1, 910-2, 913-3, 917-2) were extremely well labeled (Figs. 1–4), allowing both reconstruction of axonal arbors and quantification of dendritic spine densities. One pilocarpine EGC (906-2; 50 μm from the GC layer) had dendritic arbors that extended into both the hilus and molecular layer (ML) (Fig. 5C). The control EGC (889-3; 200 μm from the GC layer) also had dendritic arbors extending into both the hilus and ML (Fig. 5E). Although the labeling of this cell by Neurobiotin was not as robust as that of the other EGCs, it was included in the dataset since EGCs in normal tissue are relatively rare (McCloskey et al., 2006; Scharfman et al., 2007).

For the purposes of anatomical comparison, 11 GC reconstructions were obtained from the NeuroMorpho database (Tables 1, 2; available at http://NeuroMorpho.Org; Ascoli et al., 2007). These GCs were stained with horseradish peroxidase in transverse 400 μm slices, obtained from male Sprague-Dawley rats ranging in age from 47 to 58 days (Carnevale et al., 1997). They were all positioned in the GC layer and had dendritic fields that were restricted to the ML. To verify that any observed differences in the morphology of hilar EGCs versus normal GC layer GCs obtained from the NeuroMorpho database were not attributable to differences in age, handling, staining protocol, and fixation procedures between the groups, four GC layer GCs (916-1, 124-5R, 124-5L, 103-5; Tables 1, 2) from three pilocarpine-treated rats that had undergone SE were perfused at comparable ages (3.5 to 6.9 months) and processed comparably, in terms of both labeling and fixation, in relation to the hilar EGCs described above. These cells did not differ significantly from GC layer GCs obtained from the NeuroMorpho database in terms of the morphological characteristics examined, including total dendritic length per cell (post-SE GC layer GCs: 3600 ± 300 μm, normal GC layer GCs: 3700 ± 200 μm, $P = 0.7$, $n = 15$), total dendritic field size measured using 3D convex hull analysis (post-SE GC layer GCs: 5.4 ± 0.5 × 10^6 μm^3, normal GC layer GCs: 5.6 ± 0.6 × 10^6 μm^3, $P = 0.8$, $n = 15$), total number of nodes (branch points) (post-SE GC layer GCs: 15 ± 2, normal GC layer GCs: 14.2 ± 0.7, $P = 0.5$, $n = 15$), internode distance (post-SE GC layer GCs: 240 ± 20 μm, normal GC layer GCs: 263 ± 8 μm, $P = 0.3$, $n = 15$), and the number of dendrites per cell (post-SE GC layer GCs: 2.0 ± 0.4, normal GC layer GCs: 1.5 ± 0.2, $P = 0.1$, $n = 15$). Two of the four post-SE GC layer GCs had small basal dendrites, which were never observed on the normal GC layer GCs. Similarly, the apical dendritic morphology of

TABLE 2.
Anatomical Data for Each Dendrite

Cell	Type	Arbor Region	Dend #	Dend Label	Dend Type	Dend L (μm)	Node #	Vertex Analysis	Convex Hull (x10^6 μm^3)	L/Node (μm)
798-2	HE E	Hilus	4	1	B	165	0	x	0.00468	x
798-2	HE E	Hilus	4	2	B	522	3	0.5	0.126	174
798-2	HE E	Hilus	4	3	B	125	0	x	0.00468	x
798-2	HE E	Hilus	4	4	A	2208	12	1.7	2.40	184
910-1	HE E	Hilus	3	1	B	368	1	x	0.049	368
910-1	HE E	Hilus	3	2	A	3279	17	0.6	5.80	193
910-1	HE E	Hilus	3	3	B	216	1	x	0.0194	216
910-2	HE E	Hilus	2	1	A	1774	12	1.7	1.73	148
910-2	HE E	Hilus	2	2	B	724	5	1	0.227	145
913-3	HE E	Hilus	2	1	A	2448	14	1	6.20	175
913-3	HE E	Hilus	2	2	B	864	8	0.4	0.909	108
917-2	HE E	Hilus	3	1	A	2127	13	0.7	3.10	164
917-2	HE E	Hilus	3	2	B	588	3	0.5	0.239	196
917-2	HE E	Hilus	3	3	B	951	6	0.7	0.917	159
889-3	C E	H + ML	3	1	A	1405	8	1	1.03	176
889-3	C E	H + ML	3	2	A	499	2	1	0.117	250
889-3	C E	H + ML	3	3	B	125	1	x	0.00600	125
906-2	E	H + ML	3	1	A	1881	10	5	2.82	188
906-2	E	H + ML	3	2	B	145	1	x	0.00417	145
906-2	E	H + ML	3	3	B	334	2	1	0.039	167
3319201	N GCL	ML	2	1	A	1783	7	1.5	2.90	255
3319201	N GCL	ML	2	2	A	3120	11	2.5	7.45	284
3319202	N GCL	ML	1	1	A	4239	15	0.8	6.01	283
404881	N GCL	ML	2	1	A	724	2	1	0.255	362
404881	N GCL	ML	2	2	A	2143	11	2.5	2.06	195
5199202	N GCL	ML	1	1	A	4995	18	0.9	7.57	278
523886	N GCL	ML	2	1	A	1816	6	0.7	2.24	303
523886	N GCL	ML	2	2	A	1340	5	1	1.36	268
524892a	N GCL	ML	1	1	A	3704	14	2	5.51	265
524892b	N GCL	ML	1	1	A	3086	12	1.7	3.04	257
609885	N GCL	ML	1	1	A	3592	14	2	5.49	257
614882	N GCL	ML	2	1	A	2354	12	1.7	3.41	196
614882	N GCL	ML	2	2	A	827	3	0.5	0.378	276
B106885	N GCL	ML	2	1	A	2097	7	1.5	1.18	300
B106885	N GCL	ML	2	2	A	1741	7	1.5	3.22	249
B330886	N GCL	ML	1	1	A	3485	12	1.7	4.25	290
916-1	PS GCL	H + ML	3	1	A	2390	12	0.8	3.35	199
916-1	PS GCL	H + ML	3	2	A	1587	7	0.5	1.48	227
916-1	PS GCL	H + ML	3	3	B	251	1	x	0.00200	251
124-5R	PS GCL	ML	1	1	A	3694	18	2.7	5.15	205
124-5L	PS GCL	ML	2	1	A	2166	9	0.8	1.39	241
124-5L	PS GCL	ML	2	2	A	1354	4	2	0.800	339
103-5	PS GCL	H + ML	2	1	A	2699	9	0.8	2.03	300
103-5	PS GCL	H + ML	2	2	B	191	1	x	0.160	191

Anatomical data organized by individual GC dendrite. The abbreviations used are the same as those described for Table 1, except for the following: Dend Label, a designation for each individual dendrite. Dend Type, categorization of each dendrite as either basal (B) or apical (A). Vertex analysis is a quantitative measure that reflects the dendritic branching pattern (see Materials and Methods).

post-SE versus normal GC layer GCs did not differ significantly in terms of dendritic length (post-SE GC layer GCs: 2,300 ± 300 μm, normal GC layer GCs: 2,600 ± 300 μm, $P = 0.7$, $n = 22$), 3D convex hull dendritic field size (post-SE GC layer GCs: 2.4 ± 0.7 × 10^6 μm^3, normal GC layer GCs: 3.5 ± 0.6 × 10^6 μm^3, $P = 0.3$, $n = 22$), branch point number (post-SE GC layer GCs: 10 ± 2, normal GC layer GCs: 10 ± 1, $P = 0.9$, $n = 22$), internode distance (post-SE GC layer GCs: 250 ± 20 μm, normal GC layer GCs: 270 ± 10 μm, $P = 0.4$, $n = 22$), and branching pattern measured using vertex analysis (post-SE GC layer GCs: 1.3 ± 0.4, normal GC layer GCs: 1.5 ± 0.2, $P = 0.5$, $n = 22$). Therefore, for the purposes of this morphological study, the data from the two groups was pooled.

Hilar EGC physiological characteristics

As described previously (Scharfman et al., 2000), the intrinsic properties of hilar EGCs were similar to those of GC layer GCs. APs evoked at threshold using direct

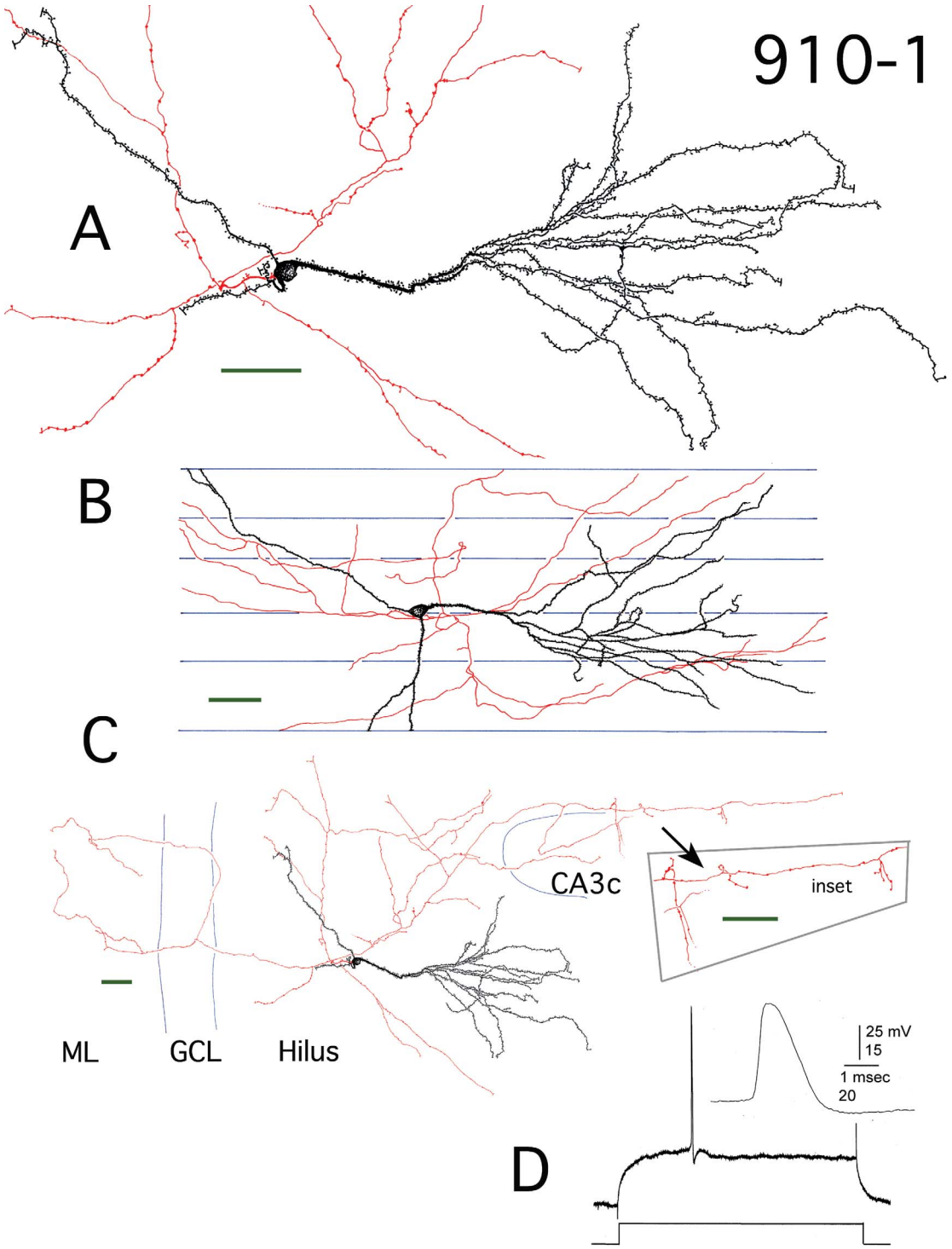

Figure 1. Reconstruction of hilar EGC 910-1. **A:** Camera lucida reconstruction of the soma, dendrites (black), and local axons (red) in the transverse plane. **B:** Longitudinal view of the cell generated by rotating and tracing the Neurolucida reconstruction. Blue lines mark the borders of individual sections. **C:** A transverse view of the complete dendritic and axonal camera lucida reconstruction. Blue lines mark subfield boundries. Inset: Mossy fiber boutons at higher magnification. ML, molecular layer; GCL, granule cell layer. **D:** Recording from hilar EGC 910-1. An action potential (AP) at threshold is shown. It was evoked using intracellular current injection at resting potential. Inset: the AP at higher gain illustrates the typical fast rate of rise and slower decay of GC APs (Scharfman, 1995a; Scharfman et al., 2000). Scale bars (green) = 50 μm.

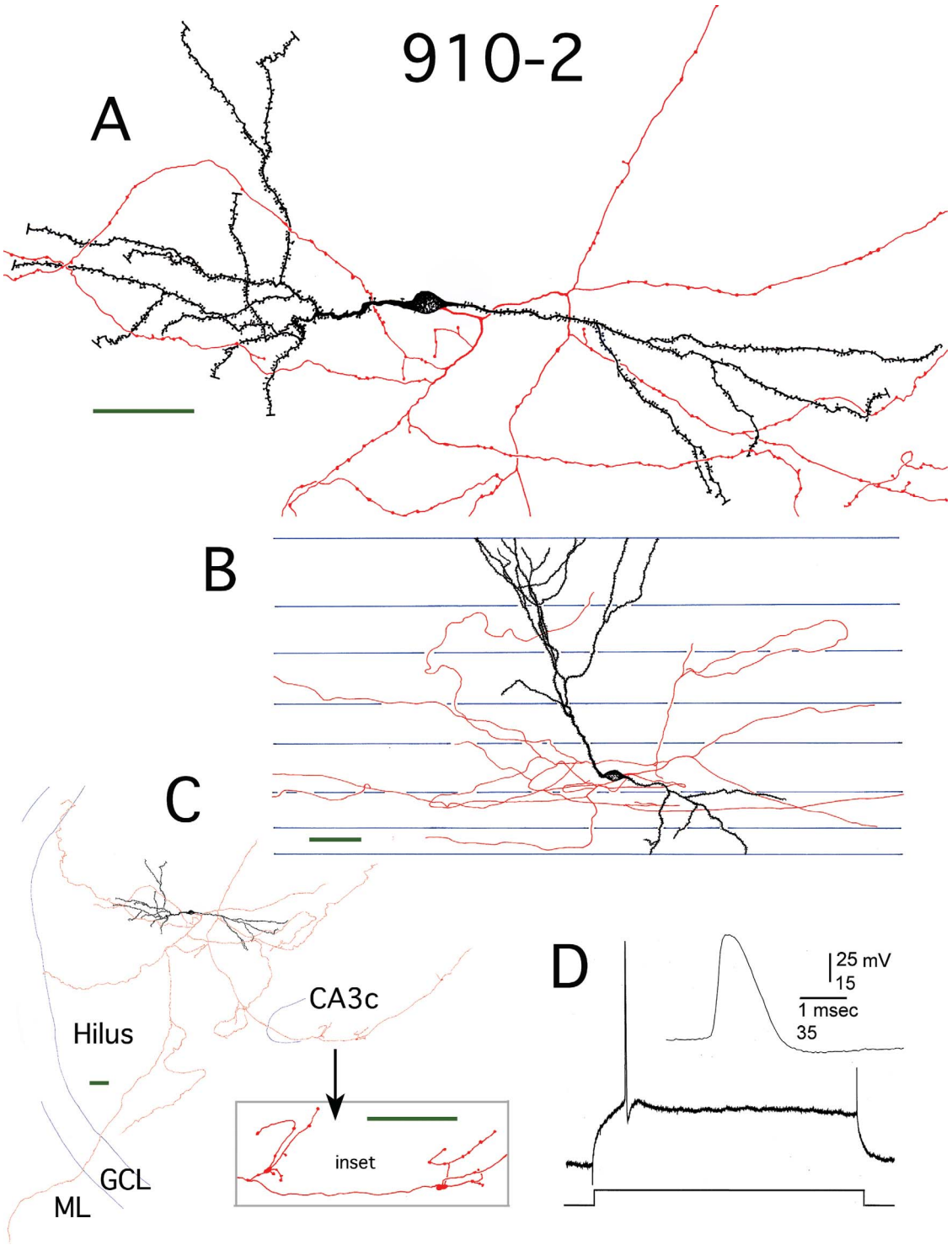

Figure 2. Reconstruction of hilar EGC 910-2. **A:** Camera lucida reconstruction of the soma, dendrites (black), and local axons (red) in the transverse plane. **B:** Longitudinal view of the cell generated by rotating and tracing the Neurolucida reconstruction. Blue lines mark the borders of individual sections. **C:** A transverse view of the complete dendritic and axonal camera lucida reconstruction. Blue lines mark subfield boundaries. Inset: Mossy fiber boutons at higher magnification. ML, molecular layer; GCL, granule cell layer. **D:** Recording from hilar EGC 910-2. An AP at threshold is shown. It was evoked using intracellular current injection at resting potential. Inset: the AP at higher gain. Scale bars (green) = 50 μm.

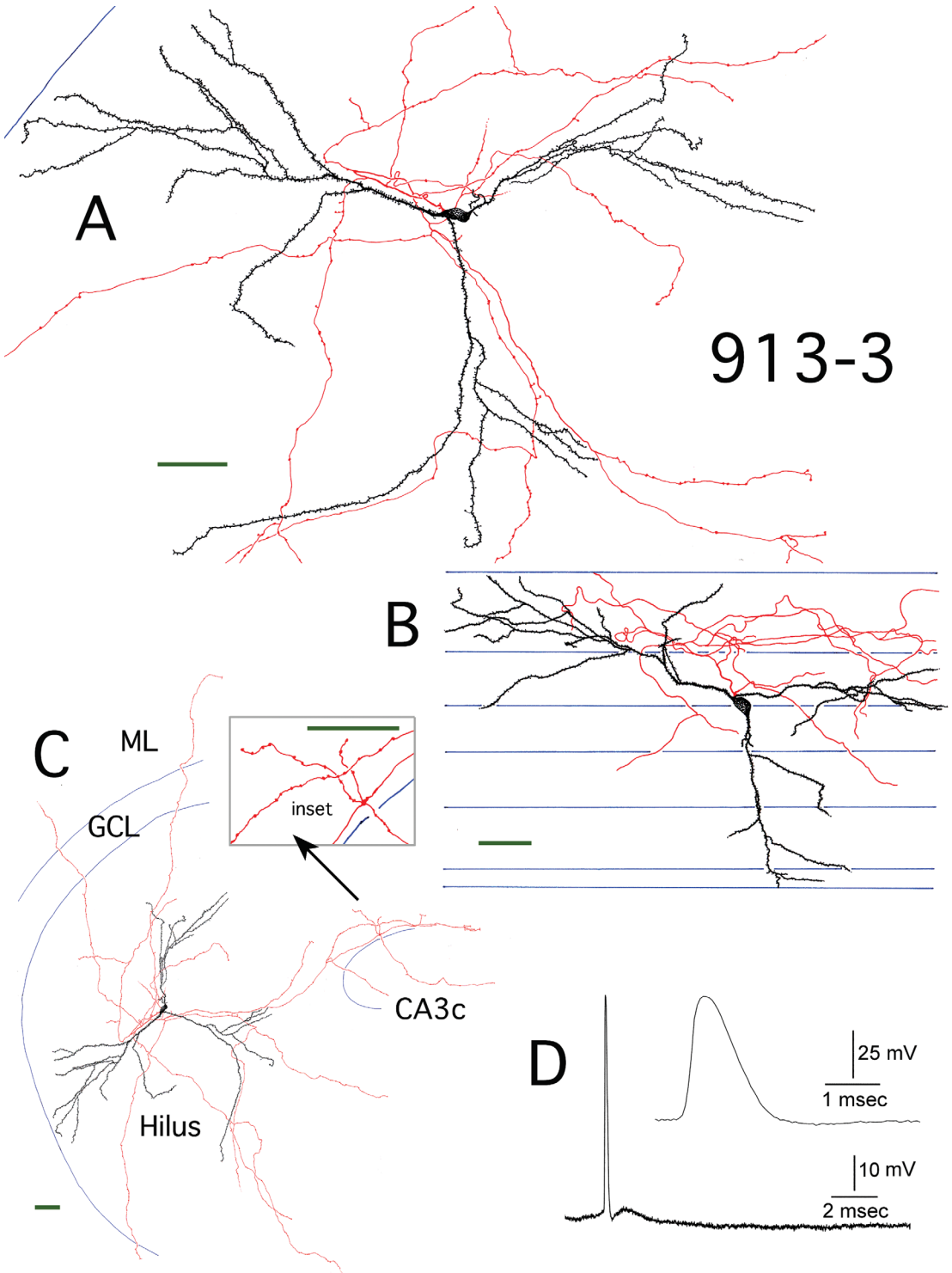

Figure 3. Reconstruction of hilar EGC 913-3. **A:** Camera lucida reconstruction of the soma, dendrites (black), and local axons (red) in the transverse plane. **B:** Longitudinal view of the cell generated from rotating and tracing the Neurolucida reconstruction. Blue lines mark the borders of individual sections. **C:** A transverse view of the complete dendritic and axonal camera lucida reconstruction. Blue lines mark subfield boundries. Inset: mossy fiber boutons at higher magnification. ML, molecular layer; GCL, granule cell layer. **D:** Recording from hilar EGC 913-3. A spontaneous AP is shown, which was evoked when the cell was depolarized to threshold. Inset: the AP at higher gain. Scale bars (green) = 50 μm.

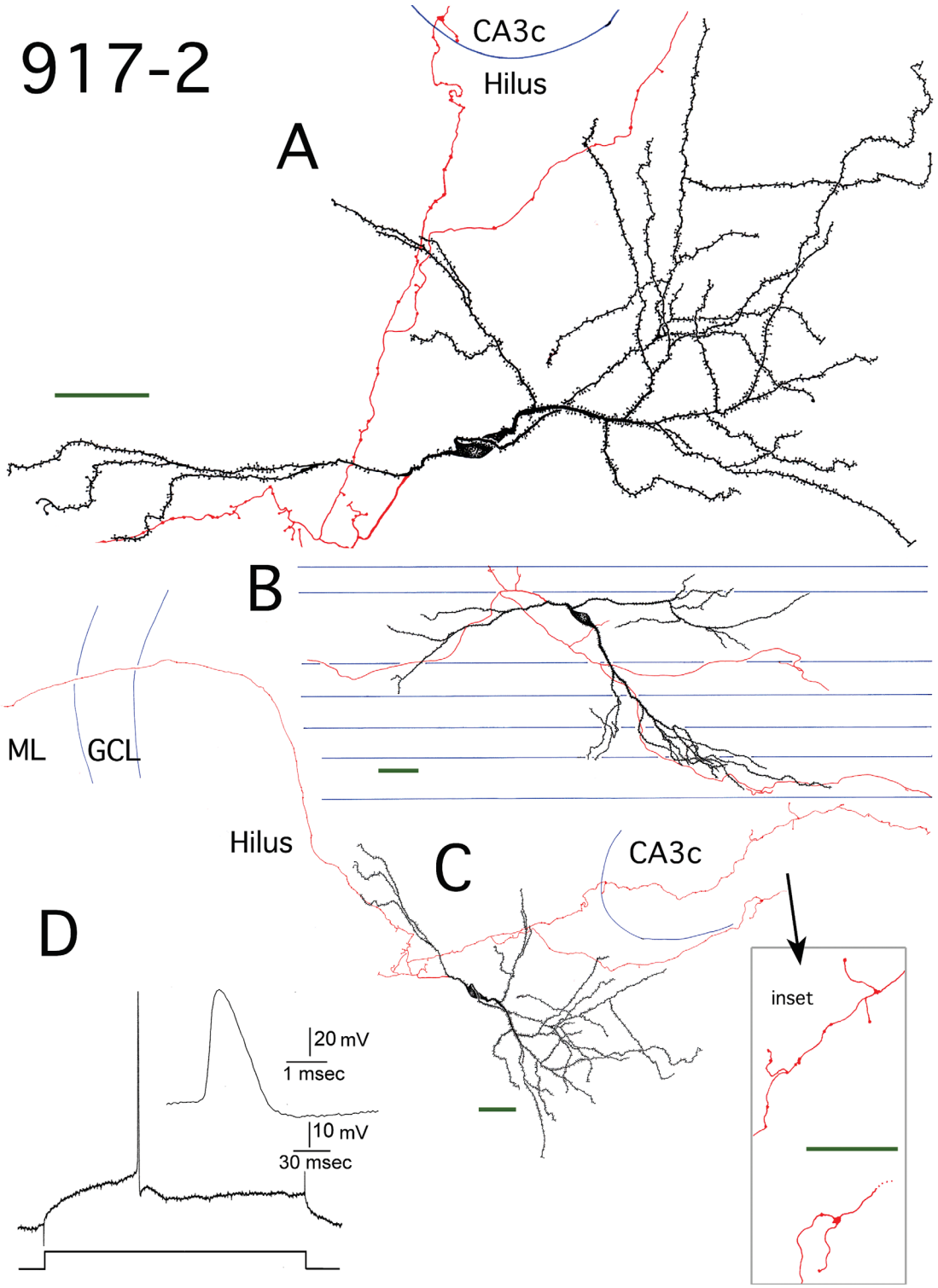

Figure 4. Reconstruction of hilar EGC 917-2. **A:** Camera lucida reconstruction of the soma, dendrites (black), and local axons (red) in the transverse plane. **B:** Longitudinal view of the cell generated from rotating and tracing the Neurolucida reconstruction. Blue lines mark the borders of individual sections. **C:** A transverse view of the complete dendritic and axonal camera lucida reconstruction. Blue lines mark subfield boundries. Inset: mossy fiber boutons at higher magnification. ML, molecular layer; GCL, granule cell layer. **D:** Recording from hilar EGC 917-2. An AP at threshold is shown, which was evoked using intracellular current injection at resting potential. Inset: the AP at higher gain. Scale bars (green) = 50 μm.

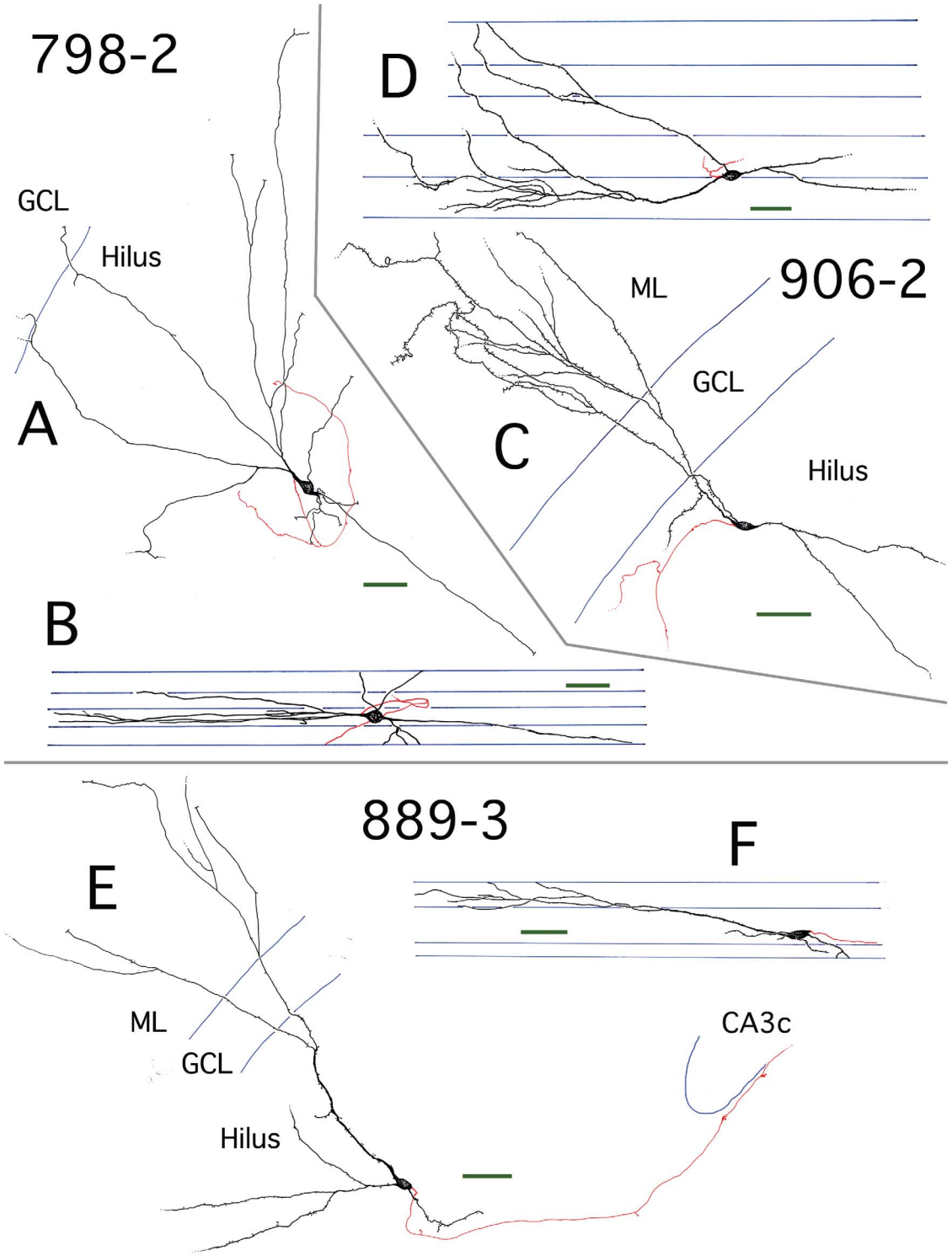

Figure 5. Transverse and longitudinal views of three hilar EGC reconstructions. **A,B:** Reconstruction of hilar EGC 798-2, presented in transverse (A) and longitudinal (B) views. Dendrites (black) were almost exclusively restricted to the hilus. Axons are shown in red. **C,D:** Reconstruction of hilar EGC 906-2, presented in transverse (C) and longitudinal (D) views. Dendrites (black) were located in both the hilus and ML. Axons are shown in red. **E,F:** Reconstruction of hilar EGC 889-3 from a nonepileptic control rat, presented in transverse (E) and longitudinal (F) views. There were dendrites (black) in both the hilus and ML. Axons are shown in red. Subfield boundaries and section borders are shown in blue. Scale bars (green) = 50 μm. GCL, granule cell layer.

TABLE 3.

Comparison of Properties of Action Potentials (APs) in Ectopic Granule Cells (EGCs)

GC number	Condition	Amp. from RMP (mV)	Amp. from thr. (mV)	AP at base (msec)	Dur. half-width (msec)	AP rise (mV/msec)	AP fall (mV/msec)	Ratio (rise/fall)	AHP peak amp (mV)
798-2	Epileptic	106	78	1.55	0.20	400	87	4.60	7.5
906-2	Epileptic	101	75	1.54	0.18	415	90	4.61	6.5
910-1	Epileptic	113	84	1.50	0.20	448	85	5.27	7.0
910-2	Epileptic	100	75	1.33	0.15	434	91	4.77	7.2
913-3	Epileptic	98	79	1.50	0.19	454	76	5.97	5.7
917-2	Epileptic	110	85	1.42	0.21	422	77	5.48	8.0
889-2	Control	105	75	1.48	0.20	452	89	5.08	6.8
Mean		105	79	1.47	0.19	432	85	5.11	7.0
SEM		40	30	0.56	0.07	163	32	1.93	2.6
N		7	7	7	7	7	7	7	7

Electrophysiological properties are listed for each hilar EGC of the study. amp., amplitude; dur., duration; AHP, afterhyperpolarization; RMP, resting membrane potential; thr., threshold; SEM, standard error of the mean. Measurements were made as previously described (Scharfman, 1995a; Scharfman et al., 2000).

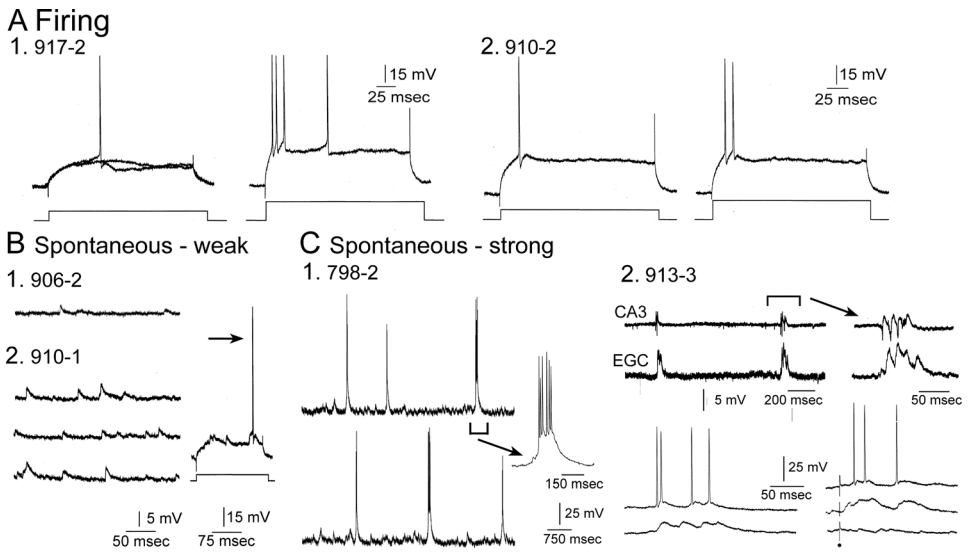

Figure 6. Comparative physiology of hilar EGCs. **A:** Representative examples of directly-evoked APs are shown for two different hilar EGCs (1,2). To evaluate spike frequency adaptation, higher currents were injected as previously described (Scharfman et al., 2000). For each cell the AP evoked at threshold is on the left and the response to increased current injection is on the right. **B:** Spontaneous activity is shown from two hilar EGCs to illustrate examples where hilar EGC spontaneous activity was relatively weak. Even though activity was subthreshold at resting potential, depolarization of the cell led to suprathreshold activity (arrow). **C:** Spontaneous activity is shown from hilar EGCs that is robust, i.e., repetitive spontaneous burst discharges. 1) A continuous recording from a hilar EGC (798-2) exhibits periodic spontaneous burst of APS. The arrow points to one of the bursts with a different temporal calibration (100 msec) to show it in more detail. 2) An extracellular recording from the CA3b pyramidal cell layer is shown (CA3; top trace) simultaneous to a recording from a hilar EGC (lower trace; expanded on the right) to demonstrate the synchrony between the hilar EGC and CA3. Lower left: A hilar EGC with repetitive burst discharges was recorded at two membrane potentials. Two spontaneous bursts of activity are shown, one at a depolarized potential where APs occurred during the burst, and one at a hyperpolarized potential where APs did not occur during the burst. Lower right: Bursts were recorded in response to stimulation of the outer molecular layer to show that they could be evoked by activation of the perforant path, as previously described (Scharfman et al., 2003). In addition, the lower right traces show that the bursts were all-or-none, because some stimuli that failed to trigger a response did not show a graded decline in amplitude, but simply failed altogether. All-or-none responses suggest that paroxysmal depolarization shifts were responsible for the bursts, as previously discussed (Scharfman et al., 2000, 2007; Scharfman, 2004).

current injection had similar amplitudes, half-widths, and slopes as previously described for hilar EGCs and GC layer GCs (Table 3). When suprathreshold currents were injected, strong spike frequency adaptation occurred (Fig. 6A).

Spontaneous activity varied among hilar EGCs (Fig. 6B,C), which also corresponds to previous descriptions of hilar EGCs (Scharfman et al., 2000). However, all hilar EGCs displayed greater spontaneous activity than normal GCs, which usually have few spontaneous potentials

when impaled with sharp electrodes (Scharfman et al., 2000, 2003). Some hilar EGCs had few spontaneous APs at resting potential, but APs occurred at depolarized potentials (Fig. 6B). Other EGCs exhibited rhythmic bursts of excitatory postsynaptic potentials and APs, with the burst onset within milliseconds of the onset of epileptiform bursts in area CA3 (Fig. 6C). Only those slices in which epileptiform bursts were recorded in area CA3 demonstrated bursts in EGCs (with the exceptions being 906-2, 910-2, and the control 889-3), similar to previous studies (Scharfman et al., 2000). When spontaneous bursts were present, bursts could also be evoked by electrical stimulation of the perforant path (Fig. 6C), as shown previously (Scharfman et al., 2003). Bursts were evoked in an all-or-none manner, consistent with an epileptiform network burst, i.e., paroxysmal depolarization shifts in pyramidal cells cause the burst (Fig. 6C) (Scharfman et al., 2000, 2003, 2007).

It is interesting to note that EGCs displayed quite similar morphology regardless of their spontaneous activity. This observation supports the hypothesis that the intrinsic properties of hilar EGCs develop primarily in an autonomous fashion, and spontaneous activity depends mostly on the emergence of network bursts in area CA3, which increase in prevalence with age after SE (Scharfman et al., 2000, 2007; Scharfman, 2004; McCloskey et al., 2006).

Hilar-exclusive EGCs have dendritic arbors that are as extensive as those of GC layer GCs

Measures of total size indicated that hilar EGCs and GC layer GCs had comparably extensive dendritic arbors. In terms of total dendritic length per cell, hilar EGCs with dendrites that were restricted to the hilus (hilar-exclusive EGCs, abbreviated hilar-ex EGCs) did not significantly differ from GC layer GCs (hilar-ex EGCs: 3,300 $\pm$ 200 μm, GC layer GCs: 3,700 $\pm$ 200 μm, $P = 0.2$, $n = 20$) (Table 1). Similarly, the total dendritic field size for these cell types, as measured using a 3D convex hull analysis (which measures the volume of a polygon formed by connecting the tips of the distal dendritic branches for each tree) did not significantly differ (hilar-ex EGCs: 4.2 $\pm$ 0.9 $\times$ 10^6 μm^3, GC layer GCs: 5.6 $\pm$ 0.5 $\times$ 10^6 μm^3, $P = 0.2$, $n = 20$). Hilar-ex EGC values tended to be somewhat smaller than those of GC layer GCs, in terms of both of these measures, but this is probably a reflection of the limits of the reconstructions. Since hilar-ex EGC dendrites were often not restricted to the transverse plane in their orientation (see below), as is usually observed for GC layer GCs, hilar-ex EGCs stained in transverse slices at times had labeled dendrites with incomplete branches, which ended at a cut surface. The percentage of branch endings that were complete (i.e., which did not end at a cut surface) was calculated for each cell (Table 1), and these values were correlated ($r = 0.57$) with total dendritic length (Fig. 7), such that the regression line, at the 100% complete point, had a y-intercept of 3,600 μm, very close to the mean value for GC layer GCs (3,700 $\pm$ 200 μm). The hilar EGC with dendritic arbors in both the hilus and ML (H + ML) (906-2, Fig. 5C) had a total dendritic length of 3,100 μm and a total convex hull volume of 3.1 $\times$ 10^6 μm^3. The control EGC (889-3, Fig. 5E) had the smallest arbor, with a total dendritic length of 2,000 μm, and a total convex hull volume of 1.2 $\times$ 10^6 μm^3.

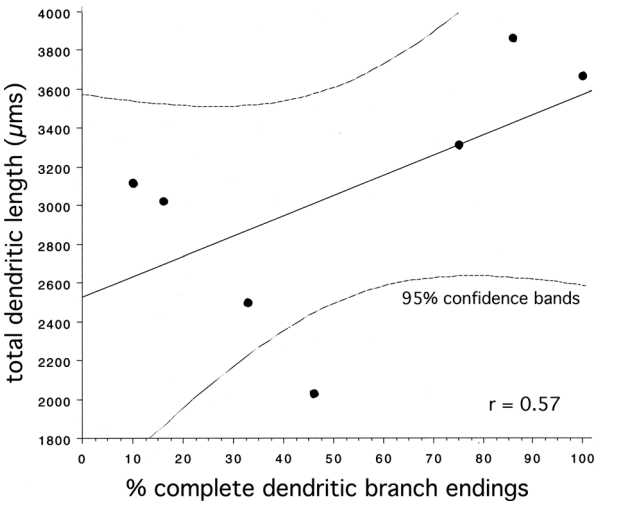

Figure 7. Plot of EGC ($n = 6$ epileptic and 1 control) total dendritic length per cell, in μm, vs. the percentage of dendritic endings that were complete (i.e., which did not end at a cut surface). These values were correlated ($r = 0.57$), such that a regression line had a y-intercept of 3,600 μm, very close to the mean value for GC layer GCs (3,700 $\pm$ 200 μm). Dashed lines reflect 95% confidence intervals.

Hilar-exclusive EGCs are topologically more complex than GC layer GCs

The dendritic arbors of hilar-ex EGCs were significantly more complex than the dendritic arbors of GC layer GCs. First, they contained significantly more branch points (nodes) (hilar-ex EGCs: 19 $\pm$ 1, GC layer GCs: 14 $\pm$ 1, $P = 0.008$, $n = 20$) (Table 1). The average internode branch distance was also significantly shorter for hilar-ex EGC dendrites in comparison to GC layer GCs (hilar-ex EGCs: 170 $\pm$ 10 μm, GC layer GCs: 258 $\pm$ 8 μm, $P < 0.0001$, $n = 20$), as one would expect from the fact that more branch points were observed within slightly smaller dendritic arbors. Visual inspection of many of these dendritic arbors (Figs. 1–4) also suggested that the path taken by individual branches was qualitatively more torturous, suggesting a less directed pattern of pathfinding.

Additionally, at a fundamental level, hilar-ex EGCs had significantly more dendrites than GC layer GCs (hilar-ex EGCs: 2.8 ± 0.4, GC layer GCs: 1.6 ± 0.2, $P = 0.003$, $n = 20$). It should be noted that two of the four post-SE GC layer GCs displayed single basal dendrites, which were never present in the normal GC layer GC population. The H + ML EGC (906-2) had four dendrites, but in terms of branching this cell more closely resembled normal GC layer GCs than hilar-ex EGCs, with 11 branch points and an average internode branch distance of 280 μm. The control EGC (889-3) had three dendrites, 16 branch points, and an average internode branch distance of 130 μm.

Dendrites of hilar-exclusive EGCs can be identified as "apical" and "basal" based on their size, complexity, and position

The dendrites of GCs within the GC layer are, by convention, identified as either apical or basal, based on their orientation. Apical GC dendrites extend into the ML, while basal GC dendrites, when they are present, project from the opposite pole of the GC cell body, into the hilus (although recurrent basal dendrites have been described; Yan et al., 2001; Dashtipour et al., 2002). These positional criteria are reinforced by differences in the size and structure of apical and basal GC dendrites, as observed in an animal model of epilepsy (Thind et al., 2008). In particular, basal GC dendrites tended to be smaller and branch less exuberantly than apical GC dendrites (although in the human, where basal dendrites are normal, these characteristics may not apply; Seress and Mrzljak, 1987). Examination of the size distribution of hilar-ex EGC dendrites (Table 2) suggests that the same classification scheme used for GC layer GCs from the epileptic rat can be applied to the EGC dendrites in this study, even though the EGCs were restricted to the hilus, and thus divorced from the usual positional criteria. Using a cluster analysis, values for total length per dendrite statistically sorted into two groups after only two iterations, demonstrating that there were two distinct populations: dendrites displaying lengths of 951 μm or less, and dendrites displaying lengths of 1,774 μm or more (Fig. 8). A similar distinction was evident using the 3D convex hull analysis to measure dendritic field volume: dendrites occupied either less than 0.92×10^6 μm^3 or more than 1.73×10^6 μm^3. Categorizing the larger group as "apical" and the smaller group as "basal," one can statistically confirm these size distinctions: apical hilar-ex EGC dendrites were significantly larger as a group than basal hilar-ex EGC dendrites, in terms of both total length (apical hilar-ex EGC dendrites: 2,400 ± 300 μm, basal hilar-ex EGC dendrites: 500 ± 100 μm, $P < 0.0001$, $n = 14$) and dendritic field volume (apical hilar-ex EGC dendrites: 3.8 ± 0.9 × 10^6 μm^3, basal hilar-ex EGC dendrites: 0.2 ± 0.1 × 10^6 μm^3, $P = 0.0003$, $n = 14$). This categorization scheme also allows further distinctions to become apparent. For instance, hilar-ex EGCs maintained a bipolar structure: they had one apical dendrite and from 1 to 3 (1.8 ± 0.4) basal dendrites, which all originated from the opposite pole of the cell body than the apical dendrite (Figs. 1–5). Apical hilar-ex EGC dendrites had significantly more branch points than basal hilar-ex EGC dendrites (apical hilar-ex EGC dendrites: 13.6 ± 0.9, basal hilar-ex EGC dendrites: 3.0 ± 0.9, $P < 0.0001$, $n = 14$). Additionally, basal hilar-ex EGC dendrites appeared to display arbors that were topologically distinct using vertex analysis. As described in Materials and Methods, vertex analysis quantifies the symmetry of branching, particularly in relation to the distribution of terminal branches. Basal hilar-ex EGC dendrites tended to display lower values than apical dendrites (basal hilar-ex EGC dendrites: 0.6 ± 0.1, apical hilar-ex EGC dendrites: 1.1 ± 0.2, $P = 0.08$, $n = 14$), suggesting that they might display a more segmental pattern of growth, with terminal branches distributed along a central, focal branch. The average internode branch distance did not differ significantly between the two groups (apical hilar-ex EGC dendrites: 173 ± 8 μm, basal hilar-ex EGC dendrites: 200 ± 30 μm, $P = 0.6$, $n = 14$), with the high level of variability displayed by basal dendrites probably being a contributing factor.

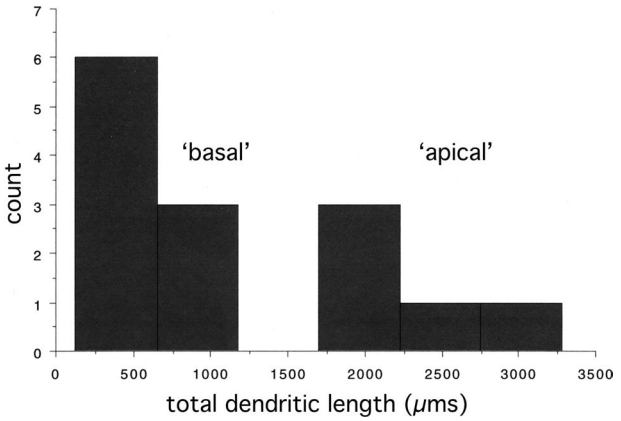

Figure 8. Classification of hilar EGC dendrites as apical and basal, based on values of dendritic length. The values for total dendritic length (in μm) for individual hilar EGC dendrites is plotted. The distribution was bimodal, suggesting that hilar EGC dendrites could be classified as either "basal" or "apical," even though they were restricted to the hilus (see text for discussion).

Apical dendrites of hilar-exclusive EGCs and GC layer GCs are quite similar in terms of both size and topology

Having defined a subgroup of hilar-ex EGC dendrites as apical, they can then be compared to the apical dendrites

of GC layer GCs. Interestingly, they were quite comparable in terms of size and structure. They displayed nearly identical mean values for total dendritic length (hilar-ex EGC apical dendrites: 2,400 ± 300 μm, GC layer GC apical dendrites: 2,500 ± 200 μm, $P = 0.8$, $n = 27$), and total dendritic field size using the 3D convex hull analysis (hilar-ex EGC apical dendrites: $3.8 \pm 0.9 \times 10^6$ μm^3, GC layer GC apical dendrites: $3.2 \pm 0.5 \times 10^6$ μm^3, $P = 0.8$, $n = 27$) (Table 2). Vertex analysis values were also similar for the two types of apical dendrites (hilar-ex EGC apical dendrites: 1.1 ± 0.2 μm, GC layer GC apical dendrites: 1.4 ± 0.1 μm, $P = 0.4$, $n = 27$). Hilar-ex EGC apical dendrites also tended to contain more branch points than GC layer GC apical dendrites, but the difference did not reach significance (hilar-ex EGC apical dendrites: 13.6 ± 0.9, GC layer GC apical dendrites: 10 ± 1 μm, $P = 0.08$, $n = 27$). The one significant structural difference that was observed was average internode branch distance: as noted for total dendritic arbors, apical dendrites in the hilus had significantly shorter internode distances than those in the ML (hilar-ex EGC apical dendrites: 173 ± 8, GC layer GC apical dendrites: 265 ± 9 μm, $P = 0.0001$, $n = 27$). The H + ML EGC (906-2) had a relatively small apical ML dendrite (total dendritic length: 1,881 μm, convex hull volume: 2.8×10^6 μm^3), and the control EGC (889-3) had two small apical (ML) dendrites (total dendritic lengths: 1,405 μm, 499 μm; convex hull volumes: 1.0×10^6 μm^3, 0.12×10^6 μm^3).

Hilar-exclusive EGC dendrites appear to display random orientations

Although hilar apical dendrites were structurally quite similar to GC layer GC apical dendrites, their spatial orientation within the DG was often radically different. All the GCs that had dendrites in the ML (normal GC layer GCs, post-SE GC layer GCs, the control EGC, and the H + ML EGC) displayed a classic, stereotypical orientation, with the apical dendrites extending towards the outer ML, and the dendritic field expanding as it approached the hippocampal fissure. The dendritic field was also relatively confined within the transverse plane. Outside of the ML, however, the dendrites extended in apparently random directions. One hilar-ex EGC (798-2, Fig. 5A,B) had an apical dendrite that extended toward the lateral blade, and was primarily confined within the transverse plane of the DG. Another (910-1, Fig. 1) had an apical dendrite that extended towards CA3c (Fig. 1C), and was not confined within the transverse plane (Fig. 1B). A third (913-3, Fig. 3) had an apical dendrite that branched almost immediately after exiting the cell body, with one secondary branch projecting towards the lateral blade (Fig. 3C), and the other extending in the opposite direction, towards CA3c (Fig. 3C). The final two hilar-ex EGCs had apical dendrites that primarily extended along the longitudinal axis of the DG, with one parallel to the edge of CA3c (917-2, Fig. 4B,C) and the other running diagonally, towards the lateral blade (910-2, Fig. 2B,C). Basal dendrites also projected in apparently random directions, running longitudinally (Figs. 1B, 3B) in the transverse plane (Figs. 4B, 5B,D) towards CA3c (Fig. 2C), or the lateral blade (Fig. 1C). Although, as mentioned, they always exited the cell body opposite the apical dendrite; in one instance (917-2, Fig. 4) one of two basal dendrites almost immediately reversed course, bending back over to the side of the apical dendrite, where it projected transversely in relation to the longitudinal path of the apical dendrite (Fig. 4B).

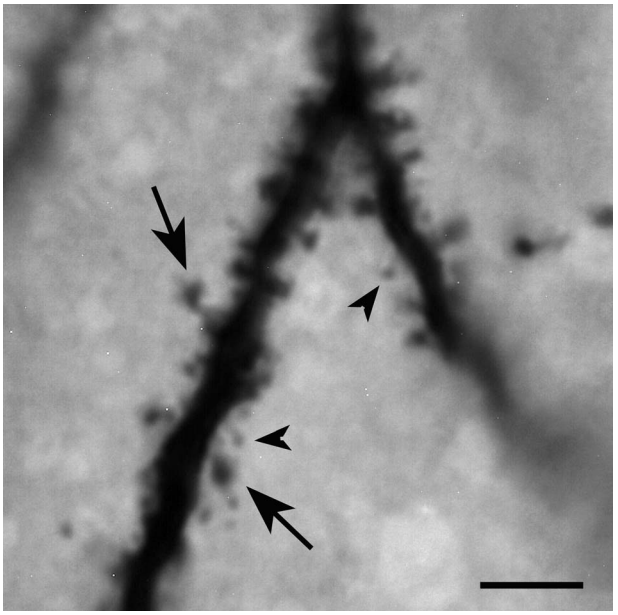

Figure 9. Example of dendritic spines of hilar EGCs. A light micrograph of an EPON-embedded dendrite from hilar EGC 913-3 with dense spine coverage. Note that the spines are quite variable in terms of their morphology, displaying both large (arrows) and small (arrowheads) spine heads. Scale bar = 5 μm.

Hilar-exclusive EGC dendrites are quite spiny

Spines on hilar-ex EGC dendrites displayed varied morphologies, with small and large heads (Fig. 9). Measurements of spine densities were collected from the four most completely filled hilar-ex EGCs (910-1, 910-2, 913-3, 917-2; Figs. 1–4) for both proximal (primary and secondary branches) and distal (terminal and next to terminal branches) portions of the dendritic arbors. Significant differences were observed in relation to branch position: proximal dendrites had higher spine densities than distal

dendrites (1.05 ± 0.05 spines/μm versus 0.88 ± 0.04 spines/μm, $P = 0.02$, $n = 21$). No significant differences were observed between hilar-ex EGC dendrites classified as either apical or basal (0.96 ± 0.04 spines/μm versus 0.96 ± 0.06 spines/μm, $P = 1.00$, $n = 21$).

Axons of hilar-exclusive EGCs innervate the same regions as GC layer GCs that have sprouted: CA3, the hilus, and the ML

As mentioned, four of the five hilar-ex EGCs (913-3, 910-1, 910-2, 917-2; Figs. 1–4) had axonal arbors that were filled well enough to justify reconstruction. Three of the four (913-3, 910-1, 910-2) had comparable lengths of labeled axon (6,784, 6,715, and 6,823 μm, respectively), while one (917-2) was less well labeled, displaying 2,127 μm of labeled axon. In this instance the axon also originated from a basal dendrite, about 40 μm from the cell body (917-2; Fig. 4A). All of the axonal arbors projected to CA3 and produced classic, large mossy fiber boutons within this region (Figs. 1–4, insets). All of the axons branched extensively within the hilus, and all sent projections across the GC layer into the ML, where varicosities were present (Figs. 1C–4C).

DISCUSSION

The results demonstrate that hilar-ex EGCs have structural characteristics that are both strikingly similar and different from GC layer GCs, regardless of condition (whether the GC layer GCs were from normal or epileptic tissue). Measures quantifying the extensiveness of dendritic arbors, such as hilar-ex EGC and GC layer GC total dendritic length and dendritic field size, were statistically indistinguishable. Observed hilar-ex EGC spine densities closely matched reported GC layer GC values (see below). In addition, hilar-ex EGCs generated the same "types" of dendrites as GC layer GCs (i.e., "apical" or "basal" dendrites), that could be distinguished by comparable morphological criteria. The axonal arbors of hilar-ex EGCs displayed the classic features GC layer GC axons, including giant mossy fiber boutons, a projection to CA3, and extensive hilar branching. They also contributed to mossy fiber sprouting, a characteristic of the DG in SE models of TLE and in many patients with TLE (Nadler, 2003; Sutula and Dudek, 2007). However, two morphological characteristics distinguished hilar-ex EGCs from GC layer GCs. First, hilar-ex EGC dendrites were more complex, with significantly more branch points, and a shorter internode distance. Second, hilar-ex EGC dendrites appeared to develop in almost random orientations, including along the longitudinal axis, in contrast to GC layer GCs, which had dendrites that were primarily restricted to the transverse axis.

It is important to note two caveats before discussing the results and their implications. First, data were generated using the pilocarpine-treated epileptic rat, which is only one of many animal models of epilepsy that simulate different aspects of TLE. Hilar EGCs are robust in this model, as well as others, where SE is used to initiate epileptogenesis, such as kainic acid-induced SE (Nakagawa et al., 2000; Scharfman et al., 2000) and electrically induced SE (Mohapel et al., 2004). Second, although data are presented for hilar EGCs with dendrites in the ML (from both normal and post-SE tissue), it should be remembered that the primary focus was hilar EGCs with dendrites confined to the hilus, i.e., hilar-ex EGCs. This subgroup, which is distinct in terms of some physiological characteristics, such as a long latency to perforant path activation (Scharfman et al., 2003), has been less well studied with regard to cellular morphology.

Hilar EGC development and environmental factors

The development of newborn neurons and their integration into the surrounding synaptic architecture presumably depends on both extrinsic environmental cues and intrinsic cellular properties. Hilar-ex EGCs, by definition, develop in isolation from the normal environment that GCs developing in the GC layer are exposed to. Additionally, potential environmental cues within the hilus are drastically altered following SE and subsequent seizures, as the region is radically restructured. In rodents this involves selective cell death (Buckmaster and Jongen-Relo, 1999; Sloviter, 1999), reactive gliosis (Wetherington et al., 2008; Seifert et al., 2010), mossy fiber sprouting (Nadler, 2003; Sutula and Dudek, 2007), and angiogenesis (Rigau et al., 2007). Indeed, it has been suggested that SE leads to a recapitulation of some developmental programs, simulating an immature state, which differs markedly from that of the normal adult DG (Szabo et al., 2000; Farooqui et al., 2001; Scharfman, 2002). It is during this period, the first 30 days after SE, when these changes, as well as further spontaneous seizures (Williams et al., 2009), are occurring, that hilar EGCs are born (Scharfman et al., 2000; Jessberger et al., 2007b). Hilar EGCs are thus exposed to an extremely abnormal environment, with fluctuating and aberrant excitability, as they develop. In this context, it is particularly surprising how much hilar-ex EGCs resemble GC layer GCs, suggesting that intrinsic factors are important determinants of their development.

Similarities between hilar-exclusive EGCs and GC layer GCs despite differences in environment

Dendritic arbor size

This resemblance is perhaps most evident in measures of total dendritic arbor size, such as total dendritic length

and field size (measured using 3D convex hull analysis), where hilar-ex EGCs and the GC layer GCs displayed statistically comparable values. Previous studies indicate that GCs display a relatively wide range of values for total dendritic length, with total length being in part dependent on the position of the soma within the GC layer (Green and Juraska, 1985; Claiborne et al., 1990). In the present study, average total dendritic length values for: 1) hilar-ex EGCs (3,300 μm); 2) post-SE GC layer GCs (3,600 μm); and 3) normal GC layer GCs (using reconstructions from the NeuroMorpho database, http://NeuroMorpho.Org; Ascoli et al., 2007; 3,700 μm) all closely corresponded to previously reported values for GC layer GCs in the normal adult rat (3,221–3,662 μm; Desmond and Levy, 1982; Claiborne et al., 1990; Rihn and Claiborne, 1990). Modeling studies that have examined the development of neuronal dendritic arbors (Luczak, 2006) provide a potential explanation for the consistency in total dendritic length between hilar-ex EGCs and GC layer GCs. Their findings suggest that there is an intrinsic constraint on the maximum size of dendritic arbors which is specific for a given cell type, which could provide a limit to competition between cells for space (Luczak, 2006).

Spine density

The average spine densities of hilar-ex EGC apical and basal dendrites in the present study (1.05 spines/μm for proximal and 0.88 spines/μm for distal dendrites) were also quite comparable to values reported in the literature for GC layer GC apical dendrites in adult male rats after SE, which range from 0.8 (Isokawa, 1998) to 1.05 spines/μm (Jessberger et al., 2007b). These post-SE spine densities represent significant reductions in relation to normal, control animal values (Isokawa, 1998; Jessberger et al., 2007b). Normal GC layer GC apical dendrite spine densities vary from 0.8 spines/μm (Turner and Schwartzkroin, 1983; Eadie et al., 2005) to 1.6 spines/μm (Desmond and Levy, 1985; Isokawa, 1998), and can depend on such factors as GC position (Desmond and Levy, 1985). Thus, hilar-ex EGCs generate and maintain GC spine densities that are typical of other GCs following SE. Additionally, it should be noted that EGCs in another environment, area CA3, also develop dense spine coverage (Szabadics et al., 2010).

Apical and basal dendrites

The most unexpected observation relating to the structure of hilar-ex EGCs was that they all had one dendrite that was distinctly identifiable as apical, even though they were totally isolated from the ML. Indeed, all hilar-ex EGC dendrites could be consistently classified as either apical or basal based on their size, polar distribution on the cell body, and branching pattern, separate from the positional distinctions that would normally categorize them. The apical dendrites were, as a group, statistically indistinguishable from GC layer GC apical dendrites, in terms of dendritic length, field size, and branching structure. Hilar-ex EGCs had from one to three basal dendrites. While basal dendrites are present on a significant portion of adult GCs in certain species, like humans and other primates (Seress and Mrzljak, 1987; Seress and Frotscher, 1990) and some bats (Buhl and Dann, 1990), in rodents they are a feature of immature GCs (Lubbers and Frotscher, 1988), virtually disappearing by maturity (Seress and Pokorny, 1981). However, after SE and chronic seizures basal dendrites are observed in adult rats and mice (Spigelman et al., 1998; Shapiro et al., 2008). Previous descriptions of GC layer GC basal dendrites in epileptic animals have suggested that basal dendrites are usually smaller and less elaborate than apical dendrites, although some basal dendrites can be relatively large (Jessberger et al., 2007b). Thind et al. (2008) reported that the basal dendrites they examined had an average total length of 612 μm, a value that closely matches that of hilar-ex EGC basal dendrites in the present study (500 μm). The number of branches was also similar, with several branches reported by Walter et al. (2007), 3.9 by Thind et al. (2008), and 3.6 in the current study. These findings further reinforce the extensive similarity between hilar EGC dendrites and those of GC layer GC dendrites in epileptic rats. EGCs that develop exclusively in area CA3 also display dendritic arbors that closely resemble GC layer GC apical dendrites (although basal dendrites are not observed) (Szabadics et al., 2010).

Axonal arbors

The pattern of hilar-ex EGC axonal arborization was remarkably consistent across the cells that were examined, and was indistinguishable from GC layer GCs following SE. Thus, all hilar EGCs had: 1) axonal projections to CA3 that displayed classic giant mossy fiber boutons at regular intervals (Blackstad and Kjaerheim, 1961; Hamlyn, 1962; Claiborne et al., 1986); 2) extensive local collaterals within the hilus that in morphology and branching pattern closely resembled those of GC layer GCs from normal rats (Claiborne et al., 1986) and epileptic rats (Sutula et al., 1992); and 3) projections into the IML that displayed varicosities, as reported for GC layer GCs in epileptic tissue (Nadler et al., 1980; Sutula et al., 1992). This finding is also in accord with previous observations, that the axons of GCs born in the adult DG project to neurons in appropriate regions (the hilus and area CA3) and form functional synapses (Toni et al., 2008).

Differences between hilar-exclusive EGC and GC layer GCs and their implications

Dendritic complexity

Although the structural features of hilar-ex EGC and GC layer GC dendrites were often quite similar, they could be distinguished on the basis of two morphological characteristics. First, hilar-ex EGC dendritic arbors were significantly more complex than those of GC layer GCs both in terms of the number of primary dendrites and the number of dendritic branch points. Second, increased complexity was also evident in the overall appearance of many hilar-ex EGC dendrites, whose branches often seemed to follow relatively crooked, torturous paths.

The propensity of hilar-ex EGCs to develop more primary dendrites than GC layer GCs could be related to previous observations that GCs located on the border with the IML had more primary dendrites (Desmond and Levy, 1982; Green and Juraska, 1985; Claiborne et al., 1990). In contrast, GCs that are positioned further from the IML usually produced a single primary dendrite that branched upon reaching the IML (Desmond and Levy, 1982; Green and Juraska, 1985; Claiborne et al., 1990). Thus, development outside of the densely packed GC layer might allow hilar-ex EGCs to produce a larger number of primary dendrites. It should also be noted that increased GC morphological variability, in terms of dendritic structure, is a hallmark of the primate (Seress and Frotscher, 1990), and human hippocampal formation (Scheibel et al., 1974) in particular.

The increased complexity of hilar-ex EGC dendrites is also particularly reminiscent of what is observed when GCs develop in hippocampal slice cultures (Zafirov et al., 1994) in the absence of their primary normal source for afferent input, the perforant path (although it should be noted that they are still contacted by presynaptic terminals; Heimrich and Frotscher, 1991). In these cultures, GC dendritic development initially parallels that of normal GCs. However, over time, the branching pattern alters, such that the number of primary dendrites increases, their polar distribution becomes less apparent, secondary and tertiary dendritic segments shorten, and take on a more twisted appearance (Zafirov et al., 1994). For hilar-ex EGCs, the absence of exposure to perforant path fibers during their development might have a similar effect on their branching pattern. In sum, these findings indicate that one of the most plastic characteristics of GC dendrites is the complexity of their branching.

Dendritic orientation

The other prominent difference between hilar-ex EGCs and GC layer GCs was the orientation of their dendritic arbors. The dendrites of hilar-ex EGCs developed in apparently random directions. This also contrasts with EGCs that are located close to the GC layer, which seem to almost invariably develop a normal GC orientation, with apical dendrites that project through the GC layer and into the ML, and basal dendrites in the hilus (Dashtipour et al., 2001; Scharfman et al., 2003). In addition, if the dendrite of a relatively distant hilar EGC (such as 889-3) did reach the GC layer, it could project normally towards the hippocampal fissure. Interestingly, the polarity of EGC dendrites was similar to GC layer GCs even if their orientation was random. Thus, for both hilar EGCs and GC layer GCs, apical dendrites emerged on the opposite side of the soma as basal dendrites. The dendrites of GCs therefore appear to develop polarity regardless of location/environment, but the orientations of the dendrites are modifiable.

Implications for DG development and function

The strong structural correspondence between hilar-ex EGCs and GC layer GCs suggests that the morphological development of GCs is autonomously controlled, primarily under the guidance of intrinsic factors. As a result, even if a GC develops in the hilus, that GC can form a somewhat normal structure, and its mossy fiber axon can find area CA3, its primary target. This argument is further supported by the recent observation that area CA3 EGCs also display “apical” dendrites with dense spine coverage, and produce classic mossy fibers (Szabadics et al., 2010). The remarkable capacity of GCs to maintain structure could allow the DG to generally preserve function, even when those GCs develop ectopically.

However, hilar-ex EGCs were distinct in several ways, such as branching complexity and dendritic orientation. These distinctions have several potential functional implications. First, the afferent input to hilar-ex EGCs and GC layer GCs is very different, with GC layer GCs receiving ML afferent input and hilar-ex EGCs receiving input primarily from afferents in the hilus. Our results suggest that it would be differences in the type and pattern of that afferent input, and its integration, not overall available dendritic surface area, that would cause functional differences between hilar-ex EGCs and GC layer GCs. In particular, the increased number of branch points and shorter internode distances of hilar-ex EGCs relative to GC layer GCs are potentially very important: dendritic bifurcations can act as nodes of integration, enhancing dendritic computational power (Mel, 1994), and potentially acting as filters for both active and passive signaling (Vetter et al., 2001; Brown et al., 2008). Furthermore, backpropagation of dendritic APs would be affected by dendritic branching.

The longitudinal orientation of some hilar-ex EGC dendritic arbors also have significant potential implications, since this orientation would allow hilar EGCs to integrate information across "hippocampal lamellae" (Andersen, 1975), instead of keeping it segregated. Disruption of lamellar processing might disrupt hippocampal function, based on anatomical and physiological arguments that it is integral to hippocampal processing (Anderson et al., 1971; Hampson et al., 1999). However, it has been suggested that the lamellar hypothesis is an oversimplification (Amaral and Witter, 1989).

Since ultimately the effects of hilar EGCs will depend on their axonal output, it is particularly important to consider the fact that hilar EGC and post-SE GC layer GC axons appear to be identical in their target regions. As a consequence, differences in input to hilar EGCs and GC layer GCs would lead to greater variance in input to target cells, such as CA3 pyramidal cells, potentially resulting in altered network function. However, homeostatic plasticity and synaptic scaling in the hippocampal formation have been well established (Leininger and Belousov, 2006; Nelson and Turrigiano, 2008; Pozo and Goda, 2010), so it is also possible that function would be normalized, particularly if hilar EGC numbers were small.

In summary, although the results suggest a high degree of GC structural preservation, even after development in the hilus, the structural differences that exist between hilar-ex EGCs and GC layer GCs could lead to an impairment of DG function, especially if significant numbers of hilar-ex EGCs were generated.

Implications for the DG in epilepsy

Impaired cognitive function

Impairments in hippocampal-dependent behavior have been observed in both animal models (Stafstrom et al., 1993) and patients with TLE (Helmstaedter, 2002; Stefan and Pauli, 2002). Since recent findings suggest that adult neurogenesis is important in pattern separation, a function attributed to the DG (Clelland et al., 2009), one might suspect that abnormal neurogenesis could contribute to impairments of hippocampal function. Support for this thesis comes from Jessberger et al. (2007a), who demonstrated that inhibition of neurogenesis after SE reduced cognitive impairment, although it is important to note that the method used had effects besides those on neurogenesis. Potschka et al. (2008) also found that cognitive function was improved by reducing neurogenesis in an animal model of epilepsy where epileptogenesis is initiated by SE, although again, the method was not completely selective for neurogenesis. Nevertheless, Potschka et al. (2008) noted that the cognitive effects of reduced neurogenesis appeared to be more robust than any effect on chronic seizures. These experimental findings have fueled an emerging discussion of postnatal neurogenesis in the DG as a potential therapeutic target to ameliorate cognitive impairment in TLE (Kuruba and Shetty, 2007; Scharfman and Gray, 2007; Scharfman and McCloskey, 2009). The results of the morphometric studies reported here add support for the hypothesis that hilar EGCs would be likely to disturb DG network function, and reducing the large numbers of hilar EGCs that develop after SE would be restorative (Scharfman and McCloskey, 2009).

Seizure generation

It is also necessary to consider the relevance of the current findings to the potential for hilar EGCs to increase DG excitability. This is critical, since it is hypothesized that the DG normally acts as an inhibitory "gate" to seizure activity, and maintaining that gate can inhibit seizures (Lothman et al., 1992; Heinemann et al., 1992; Coulter and Carlson, 2007; Hsu, 2007). The implication is that increasing DG excitability would increase seizure propagation through the hippocampal formation, leading to limbic seizures. Since past studies have shown that hilar EGCs are more excitable than normal GCs, it has been suggested that hilar EGCs might play a role in increasing DG excitability and disrupting the gate function of the DG. By promoting the propagation of seizure activity from the entorhinal cortex to the hippocampus, hilar EGCs could contribute to the generation of seizures. This suggestion is based on the observation that hilar EGCs appear to become synchronized with CA3 pyramidal cells in epileptic rat slices, creating a potential focus (Scharfman et al., 2000, 2007; Scharfman, 2004). However, these hypotheses remain to be proven.

The fact that some hilar EGCs have longitudinally oriented dendrites is relevant to the above hypotheses because, as mentioned, these dendrites could allow hilar EGCs to derive afferent input from multiple laminae. This might enable them to receive expanded convergent excitatory input from GC layer GCs, which is not otherwise possible, since mossy fiber axons are primarily confined to the transverse axis. The idea that hilar EGC dendrites, by virtue of their longitudinal projection, are optimized for receipt of mossy fiber input is supported by previous ultrastructural analyses, where it was shown that mossy fiber terminals represent the predominant source of afferent input to the shafts of EGC dendrites. On average, mossy fiber terminals comprised 67% of all terminals and occupied 40% of the surface of EGC dendritic shafts in the hilus (Pierce et al., 2005). It was noted that EGC dendrites also receive input from terminals forming symmetric (presumably inhibitory) synapses (Pierce et al., 2005), potentially from surviving interneurons. However, only 8% of all synapses on EGC dendritic shafts were symmetric (Pierce et al., 2005), suggesting that excitatory connections predominate. Recent physiological findings (Zhan et al., 2010) provide support

for this thesis: hilar EGCs display a high ratio of synaptic excitation to synaptic inhibition. Another source of excitatory input to longitudinally oriented EGC dendritic arbors could come from surviving mossy cells, since mossy cell axons also project longitudinally. Although it has been proposed that this projection primarily terminates on GC layer GCs normally (Buckmaster et al., 1996), in the epileptic rat mossy cells innervate EGCs (Pierce et al., 2007).

This pattern of predominantly excitatory, potentially strongly convergent, afferent input to EGCs is matched by a broad, divergent pattern of efferent output. EGC axons project to area CA3, the hilus, and the ML, making it likely that their activation would strongly influence both DG and CA3 network function. Such signaling could magnify the spread of excitatory activity within the structure because of the numerous recurrent excitatory circuits that these EGC connections could support. Indeed, hilar EGCs might be the "hub" cell that has been suggested to play an important role in the epileptic DG network (Morgan and Soltesz, 2008). As such, hilar EGCs could be a trigger for the DG network and not merely a contributor to mossy fiber sprouting. Since most GC layer GCs are not very active, they presumably provide relatively little excitatory drive. In contrast, hilar EGCs could act as a source of excitatory drive because of their periodic burst discharges (Scharfman et al., 2000) that originate in area CA3.

A critical component of this hypothesis is the drive provided by area CA3. Past studies of hilar EGCs have shown that CA3 exhibits synchronized epileptiform bursts in slices from pilocarpine-treated rats, and the incidence of these bursts increases in frequency with time after SE (Scharfman et al., 2000; Scharfman, 2004). Simultaneous recordings have shown that all hilar neurons burst >1 ms after these CA3 discharges, suggesting CA3 is the pacemaker, which has also been confirmed by other experiments (Scharfman, 2007). In addition to spontaneous burst discharges, the perforant path can drive CA3 to synchronously discharge, which then causes hilar neurons to burst (Scharfman et al., 2003). Therefore, hilar EGCs may be an additional source of recurrent excitation to a region that is already primed to discharge as a unit. The extent to which this network can drive seizures is likely to depend on many factors, such as the extent of cell loss in the hilus, CA3, the DG, and entorhinal cortex, which is highly variable in the pilocarpine model of TLE (Curia et al., 2008) and tissue resected from patients with pharmacoresistant TLE (Thom et al., 2002, 2009; Scharfman and Pedley, 2006; Seress et al., 2009).

CONCLUSIONS

The present study provides a quantitative description of the morphometry of hilar EGCs which sheds light on both the maturation of GCs at ectopic locations within the hilus and their integration into the DG network. The fact that many of the characteristics of GC layer GCs are conserved in hilar-ex EGCs suggests a remarkable preservation of the determinants of structure, even in an adult animal that contains extensive pathology. However, there are also aberrant structural characteristics that could contribute to cognitive impairments in the DG in epileptic rats, and their recurrent seizures.

LITERATURE CITED

Amaral DG. 1978. A Golgi study of the cell types in the hilar region of the hippocampus in the rat. J Comp Neurol 182: 851–914.

Amaral DG, Witter MP. 1989. The three-dimensional organization of the hippocampal formation. Neuroscience 31: 571–591.

Amaral DG, Woodward DJ. 1977. A hippocampal interneuron observed in the inferior region. Brain Res 124:225–236.

Amaral DG, Scharfman HE, Lavenex P. 2007. The dentate gyrus: fundamental neuroanatomical organization (dentate gyrus for dummies). Prog Brain Res 163:3–22.

Andersen P. 1975. Organization of hippocampal neurons and their interconnections. In: Isaacson RL, Pribram KH, editors. The hippocampus. New York: Plenum Press. p155–175.

Anderson P, Bliss TV, Skrede KK. 1971. Lamellar organization of hippocampal pathways. Exp Brain Res 13:222–238.

Ascoli GA, Donohue DE, Halavi M. 2007. NeuroMorpho.Org: a central resource for neuronal morphologies. J Neurosci 27: 9247–9251.

Bengzon J, Kokaia Z, Elmer E, Nanobashvile A, Kokaia M, Lindvall O. 1997. Apoptosis and proliferation of dentate gyrus neurons after single and intermittent limbic seizures. Proc Natl Acad Sci U S A 94:10432–10437.

Blackstad TW, Kjaerheim A. 1961. Special axo-dendritic synapses in the hippocampal cortex. Electron and light microscopic studies on the layer of mossy fibers. J Comp Neurol 117:133–159.

Blumcke I, Schewe JC, Normann S, Brustle O, Schramm J, Elger CE, Wiestler OD. 2001. Increase of nestin-immunoreactive neural precursor cells in the dentate gyrus of pediatric patients with early-onset temporal lobe epilepsy. Hippocampus 11:311–321.

Blumcke I, Thom M, Wiestler OD. 2002. Ammon's horn sclerosis: a maldevelopmental disorder associated with temporal lobe epilepsy. Brain Pathol (Zurich) 12:199–211.

Brown KM, Gillette TA, Ascoli GA. 2008. Quantifying neuronal size: summing up trees and splitting the branch difference. Semin Cell Dev Biol 19:485–493.

Buckmaster PS, Jongen-Relo AL. 1999. Highly specific neuron loss preserves lateral inhibitory circuits in the dentate gyrus of kainate-induced epileptic rats. J Neurosci 19: 9519–9529.

Buckmaster PS, Wenzel HJ, Kunkel DD, Schwartzkroin PA. 1996. Axonal arbors and synaptic connections of hippocampal mossy cells in the rat in vivo. J Comp Neurol 366: 271–292.

Buhl EH, Dann JF. 1990. Basal dendrites are a regular feature of hippocampal granule cells in flying fox hippocampus. Neurosci Lett 116:263–268.

Cajal SR. 1909. Histologie du Système Nerveux de l'Homme et des Vertebras. Paris: Maloine.

Carnevale NT, Tsai KY, Claiborne BJ, Brown TH. 1997. Comparative electrotonic analysis of three classes of rat hippocampal neurons. J Neurophysiol 78:703–720.

Claiborne BJ, Amaral DG, Cowan WM. 1986. The light and electron microscopic analysis of the mossy fibers of the rat dentate gyrus. J Comp Neurol 246:435–458.

Claiborne BJ, Amaral DG, Cowan WM. 1990. Quantitative, three-dimensional analysis of granule cell dendrites in the rat dentate gyrus. J Comp Neurol 302:206–219.

Clelland CD, Choi M, Romberg C, Clemenson GD Jr, Fragniere A, Tyers P, Jessberger S, Saksida LM, Barker RA, Gage FH, Bussey TJ. 2009. A functional role for adult hippocampal neurogenesis in spatial pattern separation. Science 325:210–213.

Coulter DA, Carlson GC. 2007. Functional regulation of the dentate gyrus by GABA-mediated inhibition. Prog Brain Res 163:235–243.

Curia G, Longo D, Biagini G, Jones RS, Avoli M. 2008. The pilocarpine model of temporal lobe epilepsy. J Neurosci Methods 172:143–157.

Danzer SC. 2008. Postnatal and adult neurogenesis in the development of human disease. Neuroscientist 14:446–458.

Dashtipour K, Tran PH, Okazaki MM, Nadler JV, Ribak CE. 2001. Ultrastructural features and synaptic connections of hilar ectopic granule cells in the rat dentate gyrus are different from those of granule cells in the granule cell layer. Brain Res 890:261–271.

Dashtipour K, Yan XX, Dinh TT, Okazaki MM, Nadler JV, Ribak CE. 2002. Quantitative and morphological analysis of dentate granule cells with recurrent basal dendrites from normal and epileptic rats. Hippocampus 12:235–244.

Desmond NL, Levy WB. 1982. A quantitative anatomical study of the granule cell dendritic fields of the rat dentate gyrus using a novel probalistic method. J Comp Neurol 212: 131–145.

Desmond NL, Levy WB. 1985. Granule cell dendritic spine density in the rat hippocampus varies with spine shape and location. Neurosci Lett 54:219–224.

Eadie BD, Redila VA, Christie BR. 2005. Voluntary exercise alters the cytoarchitecture of the adult dentate gyrus by increasing cellular proliferation, dendritic complexity, and spine density. J Comp Neurol 486:39–47.

Farooqui AA, Yi Ong W, Lu XR, Halliwell B, Horrocks LA. 2001. Neurochemical consequences of kainate-induced toxicity in brain: involvement of arachidonic acid release and prevention of toxicity by phospholipase A(2) inhibitors. Brain Res 38:61–78.

Frotscher M, Zhao S, Forster E. 2007. Development of cell and fiber layers in the dentate gyrus. Prog Brain Res 163: 133–142.

Gaarskjaer FB, Laurberg S. 1983. Ectopic granule cells of hilus fasciae dentatae projecting to the ipsilateral regio inferior of the rat hippocampus. Brain Res 274:11–16.

Gage FH, Kempermann G, Palmer TD, Peterson DA, Ray J. 1998. Multipotent progenitor cells in the adult dentate gyrus. J Neurobiol 36:249–266.

Golgi C. 1886. Sulla fina anatomica degli organi centrali del sistema nervoso. Milan: Hoepli.

Gong C, Wang TW, Huang HS, Parent JM. 2007. Reelin regulates neuronal progenitor migration in intact and epileptic hippocampus. J Neurosci 27:1803–1811.

Gould E, Cameron HA. 1996. Regulation of neuronal birth, migration, and death in the rat dentate gyrus. Dev Neurosci 18:22–35.

Green EJ, Juraska JM. 1985. The dendritic morphology of hippocampal dentate granule cells varies with their position in the granule cell layer: a quantitative Golgi study. Exp Brain Res 59:582–586.

Haas CA, Frotscher M. 2010. Reelin deficiency causes granule cell dispersion in epilepsy. Exp Brain Res 200:141–149.

Hamlyn LH. 1962. The fine structure of the mossy fibre endings in the hippocampus of the rabbit. J Anat 96:112–126.

Hampson RE, Simeral JD, Deadwyler SA. 1999. Distribution of spatial and nonspatial information in dorsal hippocampus. Nature 402:610–614.

Heimrich B, Frotscher M. 1991. Differentiation of dentate granule cells in slice cultures of rat hippocampus: a Golgi/electron microscopic study. Brain Res 538:263–268.

Heinemann U, Beck H, Dreier JP, Ficker JP, Stabel J, Zhang CL. 1992. The dentate gyrus as a regulated gate for the propagation of epileptiform activity. In: Ribak CE, Gall CM, Mody I, editors. The dentate gyrus and its role in seizures. Amsterdam: Elsevier. p 273–280.

Helmstaedter C. 2002. Effects of chronic epilepsy on declarative memory systems. Prog Brain Res 135:439–453.

Houser CR. 1990. Granule cell dispersion in the dentate gyrus of humans with temporal lobe epilepsy. Brain Res 535: 195–204.

Hsu D. 2007. The dentate gyrus as a filter or gate: a look back and a look ahead. Prog Brain Res 163:601–613.

Isokawa M. 1998. Remodeling dendritic spines in the rat pilocarpine model of temporal lobe epilepsy. Neurosci Lett 258:73–76.

Jessberger S, Nakashima K, Clemenson GD Jr, Mejia E, Mathews E, Ure K, Ogawa S, Sinton CM, Gage FH, Hsieh J. 2007a. Epigenetic modulation of seizure-induced neurogenesis and cognitive decline. J Neurosci 27:5967–5975.

Jessberger S, Zhao C, Toni N, Clemenson GD Jr, Li Y, Gage FH. 2007b. Seizure-associated, aberrant neurogenesis in adult rats characterized with retrovirus-mediated cell labeling. J Neurosci 27:9400–9407.

Jung KH, Chu K, Kim M, Jeong SW, Song YM, Lee ST, Kim JY, Lee SK, Roh JK. 2004. Continuous cytosine-b-D-arabinofuranoside infusion reduces ectopic granule cells in adult rat hippocampus with attenuation of spontaneous recurrent seizures following pilocarpine-induced status epilepticus. Eur J Neurosci 19:3219–3226.

Jung KH, Chu K, Lee ST, Kim J, Sinn DI, Kim JM, Park DK, Lee JJ, Kim SU, Kim M, Lee SK, Roh JK. 2006. Cyclooxygenase-2 inhibitor, celecoxib, inhibits the altered hippocampal neurogenesis with attenuation of spontaneous recurrent seizures following pilocarpine-induced status epilepticus. Neurobiol Dis 23:237–246.

Kuruba R, Shetty AK. 2007. Could hippocampal neurogenesis be a future drug target for treating temporal lobe epilepsy? CNS Neurol Disord Drug Targets 6:342–357.

Leininger E, Belousov AB. 2006. Homeostatic plasticity: comparing and contrasting cortical and hippocampal studies. A review. Crit Rev Neurobiol 18:125–134.

Li G, Pleasure SJ. 2005. Morphogenesis of the dentate gyrus: what we are learning from mouse mutants. Dev Neurosci 27:93–99.

Lorente de Nó R. 1934. Studies on the structure of the cerebral cortex-II. Continuation of the study of the ammonic system. J Psychol Neurol 46:113–177.

Lothman EW, Stringer JL, Bertram EH. 1992. The dentate gyrus as a regulated gate for the propagation of epileptiform activity. In: Ribak CE, Gall CM, Mody I, editors. The dentate gyrus and its role in seizures. Amsterdam: Elsevier. p 301–313.

Lubbers K, Frotscher M. 1988. Differentiation of granule cells in relation to GABAergic neurons in the rat fascia dentata. Combined Golgi/EM and immunocytochemical studies. Anat Embryol (Berl) 178:119–127.

Luczak A. 2006. Spatial embedding of neuronal trees modeled by diffusive growth. J Neurosci Methods 157:132–141.

Marti-Subirana A, Soriano E, Garcia-Verdugo JM. 1986. Morphological aspects of the ectopic granule-like cellular populations in the albino rat hippocampal formation: a Golgi study. J Anat 144:31–47.

McCloskey D, Hintz TM, Pierce JP, Scharfman HE. 2006. Stereological methods reveal the robust size and stability of ectopic hilar granule cells after pilocarpine-induced status epilepticus in the adult rat. Eur J Neurosci 24:2203–2210.

Mel B. 1994. Information-processing in dendritic trees. Neural Comput 6:1031–1085.

Mohapel P, Ekdahl CT, Lindvall O. 2004. Status epilepticus severity influences the long-term outcome of neurogenesis in the adult dentate gyrus. Neurobiol Dis 15:196–205.

Morgan RJ, Soltesz I. 2008. Nonrandom connectivity of the epileptic dentate gyrus predicts a major role for neuronal hubs in seizures. Proc Natl Acad Sci U S A 105: 6179–6184.

Nadler JV. 2003. The recurrent mossy fiber pathway of the epileptic brain. Neurochem Res 28:1649–1658.

Nadler JV, Perry BW, Cotman CW. 1980. Selective reinnervation of hippocampal area CA1 and the fascia dentata after destruction of CA3-CA4 afferents with kainic acid. Brain Res 182:1–9.

Nakagawa E, Aimi Y, Yasuhara O, Tooyama I, Shimada M, McGeer PL, Kimura H. 2000. Enhancement of progenitor cell division in the dentate gyrus triggered by initial limbic seizures in rat models of epilepsy. Epilepsia 41:10–18.

Nelson SB, Turrigiano GG. 2008. Strength through diversity. Neuron 60:477–482.

Parent JM, Murphy GG. 2008. Mechanisms and functional significance of aberrant seizure-induced hippocampal neurogenesis. Epilepsia 49(Suppl 5):19–25.

Parent JM, Yu TW, Leibowitz RT, Geshwind DH, Sloviter RS, Lowenstein DH. 1997. Dentate granule cell neurogenesis is increased by seizures and contributes to abberant network reorganization in the rat. J Neurosci 17:3727–3728.

Parent JM, Elliott RC, Pleasure SJ, Barbaro NM, Lowenstein DH. 2006. Aberrant seizure-induced neurogenesis in experimental temporal lobe epilepsy. Ann Neurol 59:81–91.

Pekcec A, Fuest C, Muhlenhoff M, Gerardy-Schahn R, Potschka H. 2008. Targeting epileptogenesis-associated induction of neurogenesis by enzymatic depolysialylation of NCAM counteracts spatial learning dysfunction but fails to impact epilepsy development. J Neurochem 105:389–400.

Pierce JP, Melton J, Punsoni M, McCloskey DP, Scharfman HE. 2005. Mossy fibers are the primary source of afferent input to ectopic granule cells that are born after pilocarpine-induced seizures. Exp Neurol 196:316–331.

Pierce JP, Punsoni M, McCloskey DP, Scharfman HE. 2007. Mossy cell axon synaptic contacts on ectopic granule cells that are born following pilocarpine-induced seizures. Neurosci Lett 422:136–140.

Pozo K, Goda Y. 2010. Unraveling mechanisms of homeostatic synaptic plasticity. Neuron 66:337–351.

Racine RC. 1972. Modification of seizure activity by electrical stimulation: II. Motor seizure. Electroenceph Clin Neurophysiol 32:281–294.

Ribak CE, Tran PH, Spigelman I, Okazaki MM, Nadler JV. 2000. Status epilepticus-induced hilar basal dendrites on rodent granule cells contribute to recurrent excitatory circuitry. J Comp Neurol 428:240–253.

Rigau V, Morin M, Rousset MC, de Bock F, Lebrun A, Coubes P, Picot MC, Baldy-Moulinier M, Bockaert J, Crespel A, Lerner-Natoli M. 2007. Angiogenesis is associated with blood-brain barrier permeability in temporal lobe epilepsy. Brain 130(Pt 7):1942–1956.

Rihn LL, Claiborne BJ. 1990. Dendritic growth and regression in rat dentate granule cells during late postnatal development. Dev Brain Res 54:115–124.

Sabatini DD, Miller F, Barrnett RJ. 1964. Aldehyde fixation for morphological and enzyme histochemical studies with the electron microscope. J Histochem Cytochem 12:57–71.

Sadler M, Berry M. 1983. Morphometric study of the development of Purkinje cell dendritic trees in the mouse using vertex analysis. J Microsc 131(Pt 3):341–354.

Scharfman HE. 1992. Differentiation of rat dentate neurons by morphology and electrophysiology in hippocampal slices: granule cells, spiny hilar cells and aspiny 'fast-spiking' cells. Epilepsy Res (Suppl 7):93–109.

Scharfman HE. 1995a. Electrophysiological diversity of pyramidal-shaped neurons at the granule cell layer / hilar border of the rat dentate gyrus recorded in vitro. Hippocampus 5: 287–305.

Scharfman HE. 1995b. Electrophysiological evidence that dentate hilar mossy cells innervate both granule cells and interneurons. J Neurophysiol 74:179–194.

Scharfman HE. 2002. Epilepsy as an example of neural plasticity. Neuroscientist 8:154–173.

Scharfman HE. 2004. Functional implications of seizure-induced neurogenesis. Adv Exp Med Biol 548:192–212.

Scharfman HE. 2007. The CA3 "backprojection" to the dentate gyrus. Prog Brain Res 163:627–637.

Scharfman HE, Gray WP. 2007. Relevance of seizure-induced neurogenesis in animal models of epilepsy to the etiology of temporal lobe epilepsy. Epilepsia 48(Suppl 2):33–41.

Scharfman HE, McCloskey DP. 2009. Postnatal neurogenesis as a therapeutic target in temporal lobe epilepsy. Epilepsy Res 85:150–161.

Scharfman SE, Pedley TA. 2006. Temporal lobe epilepsy. In: Gilman A, editor. Neurobiology of disease. New York: Academic Press. p 349–370.

Scharfman HE, Goodman JH, Sollas AL. 2000. Granule-like neurons at the hilar/CA3 border after status epilepticus and their synchrony with area CA3 pyramidal cells: functional implications of seizure-induced neurogenesis. J Neurosci 20:6144–6158.

Scharfman HE, Sollas AL, Goodman JH. 2002. Spontaneous recurrent seizures after pilocarpine-induced status epilepticus activate calbindin-immunoreactive hilar cells of the rat dentate gyrus. Neuroscience 111:71–81.

Scharfman HE, Sollas AE, Berger RE, Goodman JH, Pierce JP. 2003. Perforant path activation of ectopic granule cells that are born after pilocarpine-induced seizures. Neuroscience 121:1017–1029.

Scharfman HE, Goodman JH, McCloskey DP. 2007. Ectopic granule cells of the rat dentate gyrus. Dev Neurosci 29:14–27.

Scheibel ME, Crandall PH, Scheibel AB. 1974. The hippocampal-dentate complex in temporal lobe epilepsy. A Golgi study. Epilepsia 15:55–80.

Seifert G, Carmignoto G, Steinhauser C. 2010. Astrocyte dysfunction in epilepsy. Brain Res Rev 63:212–221.

Seress L, Frotscher M. 1990. Morphological variability is a characteristic feature of granule cells in the primate fascia dentata: a combined Golgi/electron microscope study. J Comp Neurol 293:253–267.

Seress L, Mrzljak L. 1987. Basal dendrites of granule cells are normal features of the fetal and adult dentate gyrus of both monkey and human hippocampal formations. Brain Res 405:169–174.

Seress L, Pokorny J. 1981. Structure of the granular layer of the rat dentate gyrus. A light microscopic and Golgi study. J Anat 133(Pt 2):181–195.

Seress L, Gulyas AI, Freund TF. 1991. Parvalbumin- and calbindin D28k-immunoreactive neurons in the hippocampal formation of the macaque monkey. J Comp Neurol 313: 162–177.

Seress L, Abraham H, Horvath Z, Doczi T, Janszky J, Klemm J, Byrne R, Bakay RA. 2009. Survival of mossy cells of the hippocampal dentate gyrus in humans with mesial temporal lobe epilepsy. J Neurosurg 111:1237–1247.

Shapiro LA, Ribak CE, Jessberger S. 2008. Structural changes for adult-born dentate granule cells after status epilepticus. Epilepsia 49(Suppl 5):13–18.

Sloviter RS. 1999. Status epilepticus-induced neuronal injury and network reorganization. Epilepsia 40(Suppl 1):S34–39.

Spigelman I, Yan X-X, Obenaus A, Lee Y-S, Wasterlain CG, Ribak CE. 1998. Dentate Granule Cells form novel basal dendrites in a rat model of temporal lobe epilepsy. Neuroscience 86:109–120.

Stafstrom CE, Chronopoulos A, Thurber S, Thompson JL, Holmes GL. 1993. Age-dependent cognitive and behavioral deficits after kainic acid seizures. Epilepsia 34:420–432.

Stefan H, Pauli E. 2002. Progressive cognitive decline in epilepsy: an indication of ongoing plasticity. Prog Brain Res 135:409–417.

Sutula TP, Dudek FE. 2007. Unmasking recurrent excitation generated by mossy fiber sprouting in the epileptic dentate gyrus: an emergent property of a complex system. Prog Brain Res 163:541–563.

Sutula TP, Golarai G, Cavazos J. 1992. Assessing the functional significance of mossy fiber sprouting. Epilepsy Res (Suppl 7):251–259.

Szabadics J, Varga C, Brunner J, Chen K, Soltesz I. 2010. Granule cells in the CA3 area. J Neurosci 30:8296–8307.

Szabo G, Kartarova Z, Hoertnagl B, Somogyi R, Sperk G. 2000. Differential regulation of adult and embryonic glutamate decarboxylases in rat dentate granule cells after kainate-induced limbic seizures. Neuroscience 100:287–295.

Takahashi RH, Milner TA, Li F, Nam EE, Edgar MA, Yamaguchi H, Beal MF, Xu H, Greengard P, Gouras GK. 2002. Intraneuronal Alzheimer abeta42 accumulates in multivesicular bodies and is associated with synaptic pathology. Am J Pathol 161:1869–1879.

Thind KK, Ribak CE, Buckmaster PS. 2008. Synaptic input to dentate granule cell basal dendrites in a rat model of temporal lobe epilepsy. J Comp Neurol 509:190–202.

Thom M, Sisodiya SM, Beckett A, Martinian L, Lin WR, Harkness W, Mitchell TN, Craig J, Duncan J, Scaravilli F. 2002. Cytoarchitectural abnormalities in hippocampal sclerosis. J Neuropathol Exp Neurol 61:510–519.

Thom M, Eriksson S, Martinian L, Caboclo LO, McEvoy AW, Duncan JS, Sisodiya SM. 2009. Temporal lobe sclerosis associated with hippocampal sclerosis in temporal lobe epilepsy: neuropathological features. J Neuropathol Exp Neurol 68:928–938.

Toni N, Laplagne DA, Zhao C, Lombardi G, Ribak CE, Gage FH, Schinder AF. 2008. Neurons born in the adult dentate gyrus form functional synapses with target cells. Nat Neurosci 11:901–907.

Turner DA, Schwartzkroin PA. 1983. Electrical characteristics of dendrites and dendritic spines in intracellularly stained CA3 and dentate hippocampal neurons. J Neurosci 3: 2381–2394.

Vetter P, Roth A, Hausser M. 2001. Propagation of action potentials in dendrites depends on dendritic morphology. J Neurophysiol 85:926–937.

Walter C, Murphy BL, Pun RY, Spieles-Engemann AL, Danzer SC. 2007. Pilocarpine-induced seizures cause selective time-dependent changes to adult-generated hippocampal dentate granule cells. J Neurosci 27:7541–7552.

Wetherington J, Serrano G, Dingledine R. 2008. Astrocytes in the epileptic brain. Neuron 58:168–178.

Williams PA, White AM, Clark S, Ferraro DJ, Swiercz W, Staley KJ, Dudek FE. 2009. Development of spontaneous recurrent seizures after kainate-induced status epilepticus. J Neurosci 29:2103–2112.

Witter MP. 2007. The perforant path: projections from the entorhinal cortex to the dentate gyrus. Prog Brain Res 163:43–61.

Yan XX, Spigelman I, Tran PH, Ribak CE. 2001. Atypical features of rat dentate granule cells: recurrent basal dendrites and apical axons. Anat Embryol (Berl) 203: 203–209.

Zafirov S, Heimrich B, Frotscher M. 1994. Dendritic development of dentate granule cells in the absence of their specific extrinsic afferents. J Comp Neurol 345:472–480.

Zhan RZ, Nadler JV. 2009. Enhanced tonic GABA current in normotopic and hilar ectopic dentate granule cells after pilocarpine-induced status epilepticus. J Neurophysiol 102: 670–681.

Zhan RZ, Timofeeva O, Nadler JV. 2010. High ratio of synaptic excitation to synaptic inhibition in hilar ectopic granule cells of pilocarpine-treated rats. J Neurophysiol 104: 3293–3304.